TERRAIN INDUCED WIND PROFILES

by

Evren Bayraktar

B.S. in Phys., Boğaziçi University, 2003

Submitted to the Institute for Graduate Studies in
Science and Engineering in partial fulfillment of
the requirements for the degree of
Master of Science

Graduate Program in Physics

Boğaziçi University

2006

ACKNOWLEDGEMENTS

I would like to express my sincere gratitude to my thesis supervisor Prof. Dr. M. Levent Kurnaz for his great support, encouragement, guidance and his understanding in my bad days.

Heartfelt thanks are for Assist. Prof. Nihat Baysal for his support and understanding throughout my studies.

I would like to thank Assist. Prof. Muhittin Mungan, and Assist. Prof. Ali Ecder for the time they have devoted to reading and commenting on my thesis.

I would like to thank Prof. Ludwig from Stanford University in U.S. for his kind gift, WOCCS. He was very helpful in my study.

I also would like to thank my friends for their assistance. Special thanks to Burcu Öztürk and Deniz Rende.

I wish to express my special thanks to my family for their belief in me.

I am especially grateful to my beloved spouse for her endless support, patience and love. This work would have been impossible without her.

ABSTRACT

TERRAIN INDUCED WIND PROFILES

In this study, the WOCSS meteorological model was used to produce three-dimensional gridded wind fields. The results simulated by WOCSS were visualized in MATLAB environment. The WOCSS model was performed using a sample data set which was supplied by Prof. Ludwig and an extracted data set from this sample by reducing the number of available data in the given data set. Then, the WOCSS model was performed on Bosphorus area. In the simulation of three-dimensional wind fields, air observation data from four surface and one upper air station were used. The surface air observation data were reported at Florya, Göztepe, Kireçburnu and Kumköy, while the radiosonde data were reported at Göztepe station. All the stations are located inside the model domain and they are spread out through the domain so to represent terrain features. WOCSS model was used to produce wind fields for the data sets belonging to 18 August, 11 October, and 10 December 1998. The model was performed on a gridded domain covering 40 km × 40 km with grid spacing 1 km. The major conclusion to be drawn is that reasonable wind analysis can be performed by using WOCSS which is a quite easy model to use and does not require large computing resources for operation. As it is always true with diagnostic models, the results may be improved by the more input wind data. However, with provided data for this study, the terrain effect on the flow was able to be simulated, and it was concluded that the dispersion or turbulence estimation models which require a three-dimensional gridded wind field can use the results of WOCSS as input.

ÖZET

ARAZİDEN ETKİLENEN RÜZGAR PROFİLLERİ

Bu çalışmada, WOCSS meteorolojik modeli üç boyutlu rüzgar alanları üretmek üzere kullanıldı. WOCSS tarafından simüle edilen sonuçlar MATLAB ortamında görselleştirildi. WOCSS modeli, Prof. Ludwig'in sağlamış olduğu veri kümesi kullanılarak uygulandı ve bu veri kümesinden daha az sayıda veri alınarak yeni bir veri kümesi oluşturuldu. Daha sonra, WOCSS modeli Boğaziçi bölgesine uygulandı. Üç boyutlu rüzgar alanları simülasyonunda, dört yer istasyonu ve bir sondaj istasyonunda gözlemlenen veriler kullanıldı. Yer istasyonu verileri Florya, Göztepe, Kireçburnu ve Kumköy'den, sondaj verileri ise Göztepe istasyonunda alındı. Bütün gözlem istasyonları, arazi özelliklerini temsil edebilecek şekilde bütün model alanına yayılarak model alanı içinde yer almıştır. WOCSS modeli 18 Ağustos, 11 Ekim, ve 10 Aralık 1998 de rüzgar alanlarının simüle edilmesinde kullanıldı. Model 40 km × 40 km'lik bir kilometre hücre aralıklarıya bölünmüş ilgi alanı için çalıştırılmıştır. En önemli sonuçlardan biri, kullanması kolay ve çok fazla bilgisayar gücü gerektirmeyen bir model olan WOCCS makul rüzgar analizleri yapabilmek için kullanılabilir. Diagnostik modellerde herzaman doğru olduğu gibi, sonuçlar daha çok rüzgar veri girdisi ile geliştirilebilinir. Ancak bu çalışma için sağlanan veriler ile akım üzeindeki arazi etkisi simüle etmek mümkün oldu ve üç boyutlu rüzgar alanı bilgisi gerektiren dağılım veya türbülans modelleri WOCCS sonuçlarını girdi olarak kullanabileceği sonucuna varıldı.

TABLE OF CONTENTS

LIST OF FIGURES

LIST OF TABLES

LIST OF SYMBOLS/ ABBREVATIONS

D	Divergence
D_t, t = 1,…,n	Divergence at the latest stage of iterations
f	Coriolis parameter
g	Gravity
h	Elevation of terrain
I	Intensity of radiation
L	Characteristic length
m	Mass
N	Brunt-Vaisala frequency
n_x, n_y, n_z	the outward positive unit normals of the directions x, y, z
P	Pressure
P_0	Pressure at the sea level
R	Universal gas constant
R_0	Rossby number
r^{-1}	Inverse distance
r^{-2}	Inverse squared distance
T	Absolute temperature
T_0	Temperature at P_0
V	Volume
$\boldsymbol{u}$	Component of wind velocity on the x-axis
u	Magnitude of wind velocity component on the x-axis
u^*	Magnitude of modified wind velocity component on the x-axis
u_0	Interpolated wind velocity component on the x-axis
u_{ND}	Magnitude of wind velocity component on the x-axis that is non-divergent
u_{RD}	Magnitude of wind velocity component on the x-axis that contributes to divergence
$\boldsymbol{v}$	Component of wind velocity on the y-axis
v	Magnitude of the wind velocity component on the y-axis
v^*	Magnitude of modified wind velocity component on the y-axis

v_0	Interpolated wind velocity component on the *y*-axis
v_{ND}	Magnitude of wind velocity component on the *y*-axis that is non-divergent
v_i	Magnitude of wind velocity component on the *y*-axis
v_{RD}	Magnitude of wind velocity component on the *y*-axis that contributes to divergence
w	Wien's constant
w_i	Magnitude of vertical component of wind velocity
w^*	Magnitude of modified wind velocity component on the *z*-axis
W_H, W_v	Horizontal and vertical weight factors
z	Elevation
z_0	Roughness Length
α_1,α_2	Gauss precision moduli values
$\delta(\ )$	First variation of the quantity in the brackets
ζ	Vorticity
ζ_t, t = 1,…,n	Vorticity at the latest stage of iterations
θ_v	Virtual potential temperature
λ	Wavelength
λ_{max}	Wavelength at which maximum energy is emitted
$\lambda(x,y,z)$	Lagrange multiplier
ρ	Density
σ	Stefan-Boltzmann's constant
ϕ	Velocity potential
Ψ	Forcing function
ω	Magnitude of angular velocity
ADI	Alternating-direction-Implicit
DEM	Digital elevation model
GTOPO30	Global 30 arc-second elevation dataset
NE	North-east
NOAA	National Oceanic and Atmospheric Administration
NW	North-west

SW	South-west
USGS	United States of Geographical Servey
UTM	Universal transverse mercator
VTMX	Vertical Transport Mixing Experiment
WOCSS	Winds on critical streamline surfaces

1. INTRODUCTION

Istanbul is a metropolis of more than 13 million residents living on both sides of the Bosphorus. Any disaster may arise accidentally or consciously involving fire, explosion, toxic or nuclear material could endanger the health and lives of millions of people.

The Bosphorus strait is considered to be one of the most difficult waterways to navigate. Approximately 4,000 ships currently pass through the narrow strait in any given month including three tankers daily. This heavy traffic through the Bosphorus undoubtedly presents substantial risks to the local environment.

In this study, WOCSS wind analysis scheme, developed by Ludwig *et al.*, (1991), was used to determine wind behavior over the Bosphorus area and how the geographical structure of Bosphorus affects the wind flow was examined. MATLAB environment was used to visualize output of WOCSS as vector plots and streamline plots. In the simplest terms, WOCSS is an air quality model that develops wind fields on a three-dimensional gridded modeling domain. Transport and dispersion models or turbulence models requires wind and temperature fields on a gridded modeling domain, which can be provided by WOCSS in the limits of real-time.

This study presents the simulation of terrain induced wind fields over Bosphorus and provides a basis for studying plume behavior and of estimation low turbulence areas for Bosphorus area.

2. THE ATMOSPHERE

The atmosphere is a thin film of fluid on the spherical Earth under the influence of gravity, Earth's rotation and differential heating by solar radiation. In this section, the chemical composition of the atmosphere and key physical properties of air are described. The equation of state of air (the connection between pressure, density and temperature) are discussed.

2.1. TEMPERATURE

2.1.1. The Heat and The Temperature

The atmosphere can be considered as a gigantic engine whose end products are winds and all other weather processes. The required energy for this engine is provided by the Sun as heat. The heat is absorbed by the atmosphere in several ways. Some of the heat energy is received directly from the Sun and indirectly from the Earth surface. Also, while water vapor is condensing it gives some part of its energy to atmosphere as heat.

Radiation is practically an instantaneous process since radiation is in the form of an electromagnetic wave that moves with a speed (not in vacuum) close to speed of light. Radiation is most effective at relatively high temperatures but it is also important at the temperatures prevailing on the Earth. A perfect radiator is called black body. Black body completely absorbs all wavelengths of incident energy and it radiates with the greatest possible effectiveness at any temperature. There are two physical laws involving radiation that are especially important in meteorology. One of these relates intensity of radiation to temperature, is called Stefan-Boltzmann's law. This law states that the intensity of radiation from a radiating body is proportional to the forth power of its temperature.

$$I = \sigma T^4 \tag{2.1}$$

where I is the intensity of radiation, T is the absolute temperature and σ is Stefan-Boltzmann's constant.

The other law, which relates the wavelength of radiation emitted by a black body to the temperature is called Wien's displacement law. The Wien's displacement law follows from Planck's formula,

$$E(\lambda,T)d\lambda = c_1\lambda^{-5}\left(\exp\frac{c_2}{\lambda T}-1\right)d\lambda \tag{2.2}$$

where λ is wavelength, c_1 and c_2 are constants. Wien's formula simply gives a relation between the wavelength of radiation and temperature,

$$\lambda_{\max}T = w \tag{2.3}$$

where $\lambda_{\max}$ is the wavelength at which the maximum energy is emitted, w is the Wien's constant.

Due to an extremely large mean distance between the Sun and the Earth, the Sun'ss rays hitting the Earth are almost parallel. Measurements indicate that the radiant flux, received from the Sun outside the Earth's atmosphere is remarkably constant. The so-called solar constant, 1367 W/m^2, defines the average amount of energy received in a unit of time on a unit area perpendicular to the path of the radiation outside the atmosphere at the average distance of the Earth's orbit around the Sun. This value fluctuates with a few percent resulted especially from the change of Sun-Earth distance in the orbit during a year (Schmid, 1995). The radiation from the sun covers a nearly continuous spectrum from 1500 A to over 40000 A but the radiation intensity is maximum at a wavelength of about 4900 A in the blue green part of the visible light spectrum.

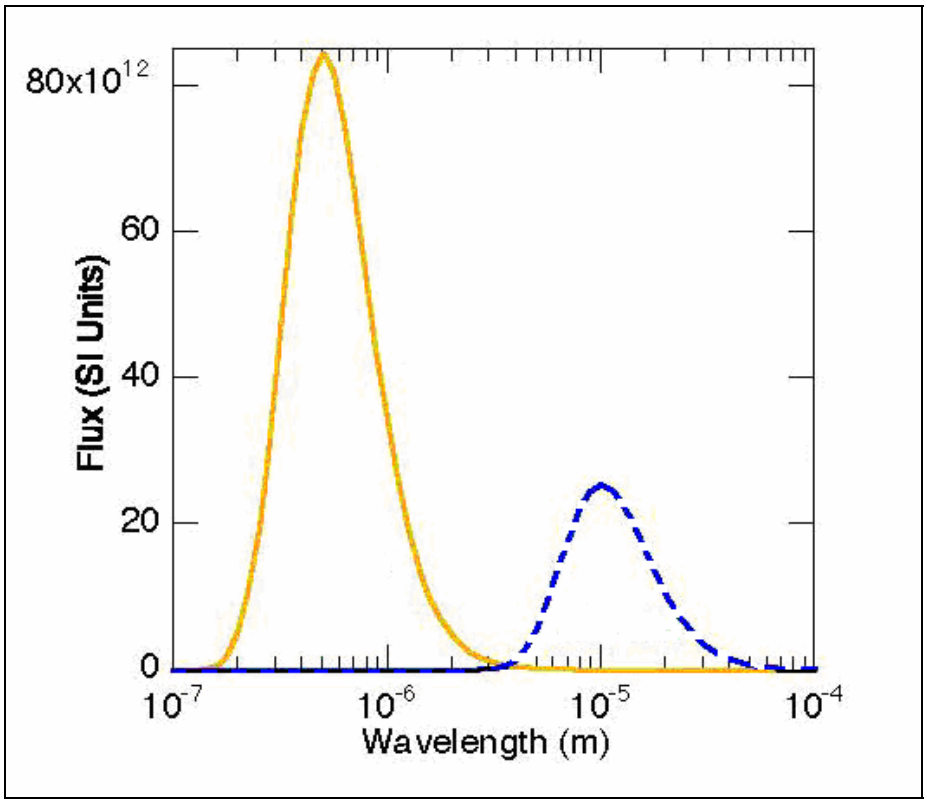

Figure 2.1. The solar (solid line) and terrestrial (dashed line) radiation (Downs R., 2005)

Considering the Sun as a black body, from Wien's formula, average surface temperature of the Sun can easily be calculated.

$$T = \frac{w}{\lambda_{\max}} = \frac{2940}{0.49} = 6000^{o} K \qquad (2.4)$$

The solar radiation, from this perfect radiator at 6000^{o} K, strikes the Earth and is disposed of in a number of different ways. 33% of it is immediately reflected back to space, 9% and 27 % are scattered respectively to the space and down to the Earth's surface by the atmosphere, 27% and 15% are absorbed respectively by the Earth's surface and the atmosphere. Absorption of solar radiation is caused mostly by atmospheric gases and partly by clouds. Ozone (O_3) is primarily responsible for the UV radiation. Depletion of ozone layer has therefore a harmful effect on the Earth's biological systems. Water vapor (H_2O) results in the absorption bands around infrared and absorbs longer wavelengths together with carbon dioxide (CO_2) (Wenham, *et al*., 1998). The Earth is bathed in solar radiation and absorbs much of it. To maintain equilibrium it must warm up and radiate

energy away at the same rate as it is received. Temperature of the Earth is accepted to be around 300º K and a body at this temperature radiates energy in the infrared. But the atmosphere is strongly absorbing at these wavelengths due to the presence of triatomic molecules principally, H_2O and CO_2, which absorb and emit in the infrared raising the surface temperature above that of the emission temperature, a mechanism that has become known as the greenhouse effect. When a thin cloud layer permits insolation to pass through but stops outgoing long-wave radiation so that the regions warm up.

After Sun's radiation reaches the Earth's surface it is absorbed and warms up the Earth. This could go on and on and the Earth gets hotter and hotter but surface of the Earth radiates approximately as a back body. Since the mean temperature near the surface is almost 300^{o}K, Wien's law indicates that,

$$\lambda_{\max} = \frac{w}{T} = \frac{2940}{300} \cong 10\,\mu m \tag{2.5}$$

The maximum of radiation is at a wavelength close to 10 μm. This value is far from the maximum of incoming solar radiation of nearly 0.5 μm.

As a result, substances whose absorption is unimportant for short-wave solar radiation may become significant absorbers and emitters of the long-wave terrestrial radiation. The dominant constituents of the atmosphere in this respect are water vapor, carbon dioxide, and ozone. From roughly 5 to 8 μm there is a strong absorption band of H_2O. Beyond the 8 μm the absorption band of H_2O becomes smaller up to about 13.5 μm except for a strong narrow band due to O_3 at 9.6 μm which masks a weaker band of CO_2 near 10 μm. The absorption of CO_2 begins at 13.5 μm and extends to 17 μm. Although the atmosphere again becomes transparent beyond 17 μm until the rotation band of H_2O appears at 24 μm and beyond, the amount of terrestrial radiation at these wavelengths is secondary in importance and 14 μm is frequently taken to be the cut-off point beyond which the atmosphere may be thought of as completely opaque (Hess,1966).

The gained heat by the atmosphere is distributed non-uniformly. Since shape of the Earth is geoids, Earth's rotational axis is tilted by 23.45^{o} angle and Earth is rotating around its own axis and on an elliptic orbit around the sun, the absorbed energy cannot be uniform everywhere. However, heat is transferred from high temperature areas to low temperature areas for uniform distribution.

There are three main ways of heat transfer. Radiation is one of them, which was discussed above, does not need a medium to transfer energy. However, the rest two can not transfer heat in absence of matter. Conduction is a relatively slow process. It requires that the activity of each molecule in a substance be speeded up, and that this increased energy be transferred to its neighbor. If the temperature difference between the source of heat and the place where it is going is large, it will move rapidly. If it is small, it will move slowly. In the atmosphere, conduction is of relatively importance because the temperature differences are too small, distances are too great, and the conductivity is too poor. During an entire night, in fact, cooling by conduction alone will affect only the lowermost five or six feet of the atmosphere (Taylor, 1954). Convection operates much faster than conduction in atmosphere. Convection implies that a volume of air rises in a gravitational field because of a local elevation of temperature which causes a reduction in density and hence an upward force or buoyancy (Sutton, 1953).

2.1.2. Temperature Gradient

Temperature gradient at any point is the rate of change of temperature with distance in any given direction. The direction can be whether horizontal or vertical.

If the chosen direction is vertical, the temperature can be expressed as a function of height above the surface level. This function is called temperature profile. It is a well known fact that, in general, temperature decreases with height, but this simple statement must be modified for conditions near the ground. On a warm clear day, temperature falls very rapidly with height in the surface layers, however after the sunset, especially with clear sky, the temperature of the air usually increases from the ground upward (Sutton, 1953).

In the atmosphere, the temperature decreases on the average at the rate of about 6.5^{o}C per kilometer up the tropopause. The average rate of decrease of temperature in the vertical is called lapse rate. If the temperature remains constant with elevation, the lapse rate is said to be isothermal; if the temperature increases aloft the lapse rate is negative and a temperature inversion exists.

When air moves vertically as it does when it rises over a mountain, or when one air mass runs up over another or when it sinks, its temperature changes as required by the first law of thermodynamics (for an isolated system, when a mechanical work is transformed into heat or heat into work, the amount of work is always equivalent to the amount of heat) and the general gas law.

$$PV = \rho RT \tag{2.6}$$

Whenever the pressure of a parcel of air changes and no heat is added or subtracted, in other words when a parcel of air under goes an adiabatic processes, the temperature of this air parcel changes as follow:

$$\frac{T}{T_0} = \left(\frac{P}{P_0} \right)^{0.288} \tag{2.7}$$

Where T_0 is the absolute temperature at the pressure P_0, and T is the absolute temperature at pressure P. Most small scale, short-term weather processes approach adiabatic conditions unless water is evaporated or condensed, because the transfer of heat by conduction and radiation is slow and heat transfer by mixing is ineffective on a small scale.

As it was explained, there is a close relation between temperature and pressure. Since the air temperature is so sensitive to pressure changes, it has been found convenient to refer all temperatures in the free atmosphere to a standard pressure. When an observed temperature T, at a pressure P, is regulated to standard pressure of 1000 millibars with the Equation 2.7, the resultant temperature is called potential temperature.

2.1.3. Variation of Temperature

The diurnal variation of temperature in the lowest layers of the atmosphere is a commonplace feature of daily life. In clear weather, the temperature profile in the first hundred meters exhibits a marked diurnal variation. However, in overcast conditions, the diurnal variation of temperature almost entirely disappears, and whose character is best revealed by examining the temperature profile (Sutton, 1953).

The average daily temperature reaches a low point just after sunrise and a high point about midafternoon. Being temperature minimum in the morning is trivial to explain, since as soon as the Sun rises, the ground starts to warm up. However, why the maximum temperature occurs several hours after noon requires a little explanation. During whole year the daily maximum temperatures occurs in midafternoon but the time of maximum heat reception takes place few hours ago. Why this situation occurs can be understood from Figure2.2.

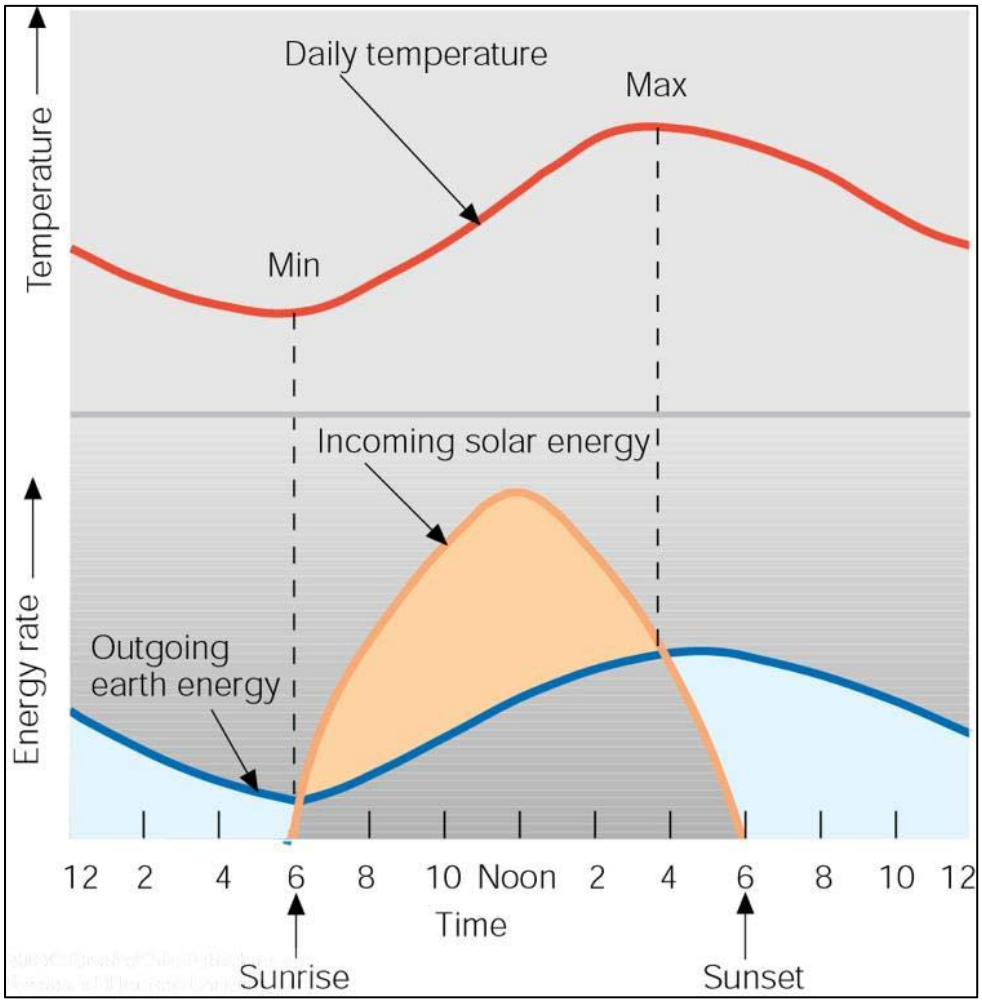

Figure 2.2. The daily energy budget of Earth

The incoming curve shows how the insolation varies from zero at morning to maximum at noon and zero at sunset again in a normal sine wave pattern. The outgoing curve shows how the long-wave radiation emitted by the earth varies from a minimum (at the time of minimum temperature) right after sunrise to a maximum in midafternoon (at the time of maximum temperature). The curve of outgoing radiation is thus also a curve of temperature variation, since the radiation emitted is directly proportional to the fourth power of the absolute temperature (Equation 2.1). The lag is caused by the heat that is stored up in the Earth's surface and lowermost atmosphere and then slowly emitted after the peak of solar radiation passed. Thus, even when the solar radiation is decreasing between noon and midafternoon, the total heat being radiated by the earth increases for a time, with the stored up heat being added to the incoming heat.

This characteristic variation of daily temperature applies everywhere except in Polar Regions where the Sun's altitude does not change much. The diurnal temperatures range is greatest at low altitudes and at continental locations. It is least at high latitudes and at maritime locations. Therefore, it is worth to explain temperature distribution over the Earth.

The highest temperatures are observed near the Equator whereas the lowest temperatures are found near the Poles. Then it is obvious that the latitude affect is primary factor in temperature distribution. The other two factors of greatest importance are the distribution of land and water, and the topography. Water bodies as long as they remain unfrozen are great moderators of the temperature because of water's high specific heat capacity.

Topographical effects are another factor of temperature distribution. For example, mountain ranges affect the temperature in their vicinity in several ways: they act as obstacles to the flow of cold air near the surface, and they often set up the conditions for warm, Chinook winds or cold, bora type winds.

In order to see all results of these effects and to have a general idea on the temperature distribution over the Earth, Figure 2.3 will be helpful.

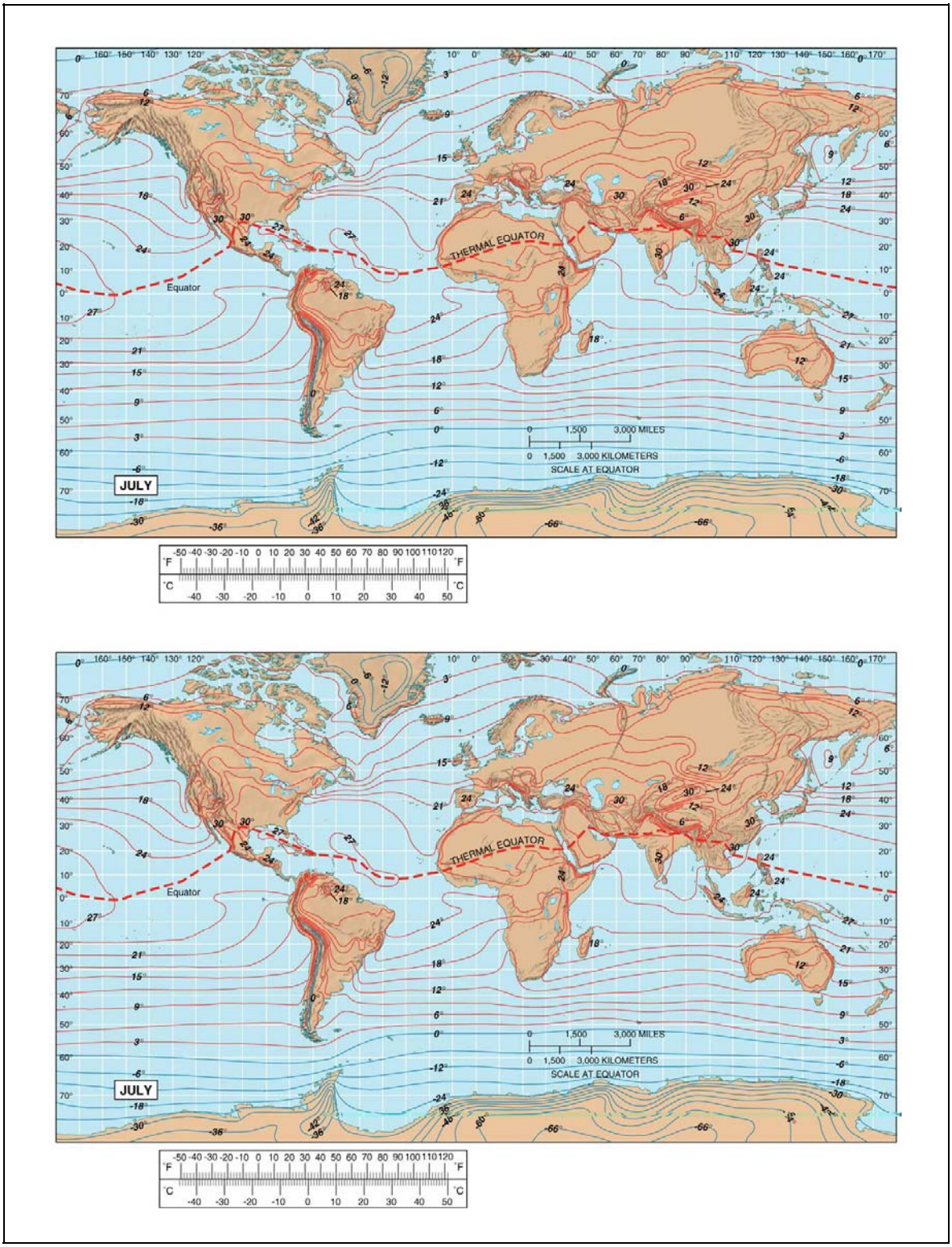

Figure 2.3. The average temperature of January and July

The figure obviously show that the highest temperatures are observed at the Equator and lowest temperatures are found at the Poles. The coldest and warmest temperatures

occur in winter and summer respectively occurs in hinterland regions. The isotherms in southern hemisphere are much more regular than the ones in northern hemisphere due to large percentage of ocean in the southern hemisphere. And whenever an isotherm crosses the continent after ocean, a distortion of isotherm is observed. Influence of high mountain ranges can be seen clearly in North America (Rocky Mountains), South America (Andes), and Asia (Himalayas). The effect of Andes and Rocky Mountains are more obvious than the Himalayas. Since Andes and Rocky Mountains are oriented north-south direction, they deflect the isotherms strongly. However, the effect of the Himalayas is mainly to cause a packing of the isotherms in their vicinity without much deflection. This is because they trend east-west, in line with the prevailing winds.

2.2. PRESSURE

In order to understand the effect and related factors of pressure, two of the mechanical laws which are followed by atmospheric gases, should be examined. The first one is Boyle's Law states that at a constant temperature, the volume (V) of a mass of gas varies inversely as it is pressure (P).

$$P = \frac{K_1}{V} \tag{2.8}$$

Where K_1 is a constant. The later one is Charles's Law which states that at a constant pressure, volume varies directly with absolute temperature (T).

$$V = K_2 T \tag{2.9}$$

These laws imply that the three qualities of pressure, temperature and volume are completely interdependent, such that any change in one, or both of them will cause a compensating change to occur in one, or both, of the remainder (Barry and Chorley, 1968).

2.2.1. Atmospheric Pressure

In meteorology much attention is given to the pressure of the air both at the surface of the Earth and aloft. Detailed and general maps of the pressure distribution are drawn. First it should be pointed out clearly that pressure by itself is not the point of interest instead pressure is often a key to understand and to predict weather processes.

To be able to study with atmospheric pressure data, the raw data should be evaluated. The pressure variations at individual stations may be presented as daily, monthly or yearly averages according to purpose of usage. For instance, in order to study wind structures it is useful to plot the pressure at different stations all measured at the same time in other words to obtain a synoptic chart which are widely used in meteorology.

In using synoptic pressure charts it is first necessary to deal with pressures at the same level if we are interested in comparing pressures at stations any distance apart. The most convenient reference level for many purposes is sea level. So the atmospheric pressures at a number of stations, all made at the same time, are reduced to sea level. The formulation of the pressure reduction is quite simple, first Laplace equation states that

$$\frac{dP}{dz} = -\rho g \tag{2.10}$$

Where z is the elevation, ρ is the density and g is the gravity. Inserting density in terms of temperature, which can be easily obtained from the equation of state Equation 2.6, into the Laplace equation will yield

$$\frac{dP}{P} = -\frac{g\,dz}{RT} \tag{2.11}$$

If we assume that temperature (T) and gravity (g) is constant through z axis Equation 2.11 will result as

$$\ln P_0 - \ln P = \frac{gz}{RT} \tag{2.12}$$

Where P_0 is the pressure at the sea level and P is the pressure at the height z. So the measured pressures above the sea level are reduced according to Equation 2.12.

2.2.2. Atmospheric Pressure Variations

The atmospheric pressure at a given locality varies continually. This variation is made up of some rather regular oscillations superimposed on irregular components caused by the passage of winds.

Diurnal pressure variations are the kind of the regular variations. The average march of pressure during the day can be computed by averaging the pressure at each hour for a long period so that pressure changes due to storm passages are eliminated. When this is done, the resulting march of pressure shows a regular trace with well-marked times of high and low pressure. The primary cause of this diurnal or daily variation is the alternate heating and cooling of the earth's atmosphere by the Sun. This cause a rhythmic expansion and contraction of the atmosphere that starts the pressure to fluctuating. If these were the only processes, there would be a period of minimum pressure about the time of maximum temperature and a period of maximum pressure about the time of minimum temperature. It happens though, that the atmosphere itself has a free period of oscillation of about 12 hours where as temperature oscillation has a period of 24 hours. This type of pressure oscillation is typical of sea level stations in the tropics. Stations near sea level in high latitudes show smaller total variation and less regularity. Mountain stations often show unusual daily pressure variations.

Above the regular diurnal pressure variations are mentioned but there are also irregular daily pressure variations. The atmospheric pressure at a given locality usually shows continual variations from hour to hour and from day to day that are caused by the passage of large scale pressure systems. These irregular variations are most pronounced in

the middle latitudes where the storm activity reaches a maximum. In the tropics, the barograms show little novelty unless a tropical storm comes along.

After the daily pressure variations, it will be worth to explain annual pressure variation. In general, the range of annual pressure variation is smallest at the Equator, and increases somewhat in the tropics. In the middle and high latitudes, there is no relation between latitude and annual pressure variation. In general, pressure is high in winter over the continents and high in summer over the oceans. Along the coast, all kind of intermediate types of variation are found.

2.2.3. World Wide Pressure Distributions

The atmospheric pressure has different patterns on the two hemispheres. In order to understand these pressure patterns and pressure distribution over the earth, first pressure systems should be studied.

There are two pressure systems as low-pressure and high-pressure systems. Areas of low pressure systems are characterized at ant level by centers or lines of low pressure surrounded by relatively higher pressure. A center of low (high) pressure surrounded on all sides by higher (lower) pressure is called a Low (High). The nature of a Low in the vertical depends on the temperature distribution within it so the nature of a High does. If the temperature is lowest (highest) at the center, the Low (High) will increase in intensity aloft. If the temperature is highest (lowest) at the center, the Low (High) will decrease in intensity aloft. So, high-pressure and low-pressure systems are classified as cold-core and warm core.

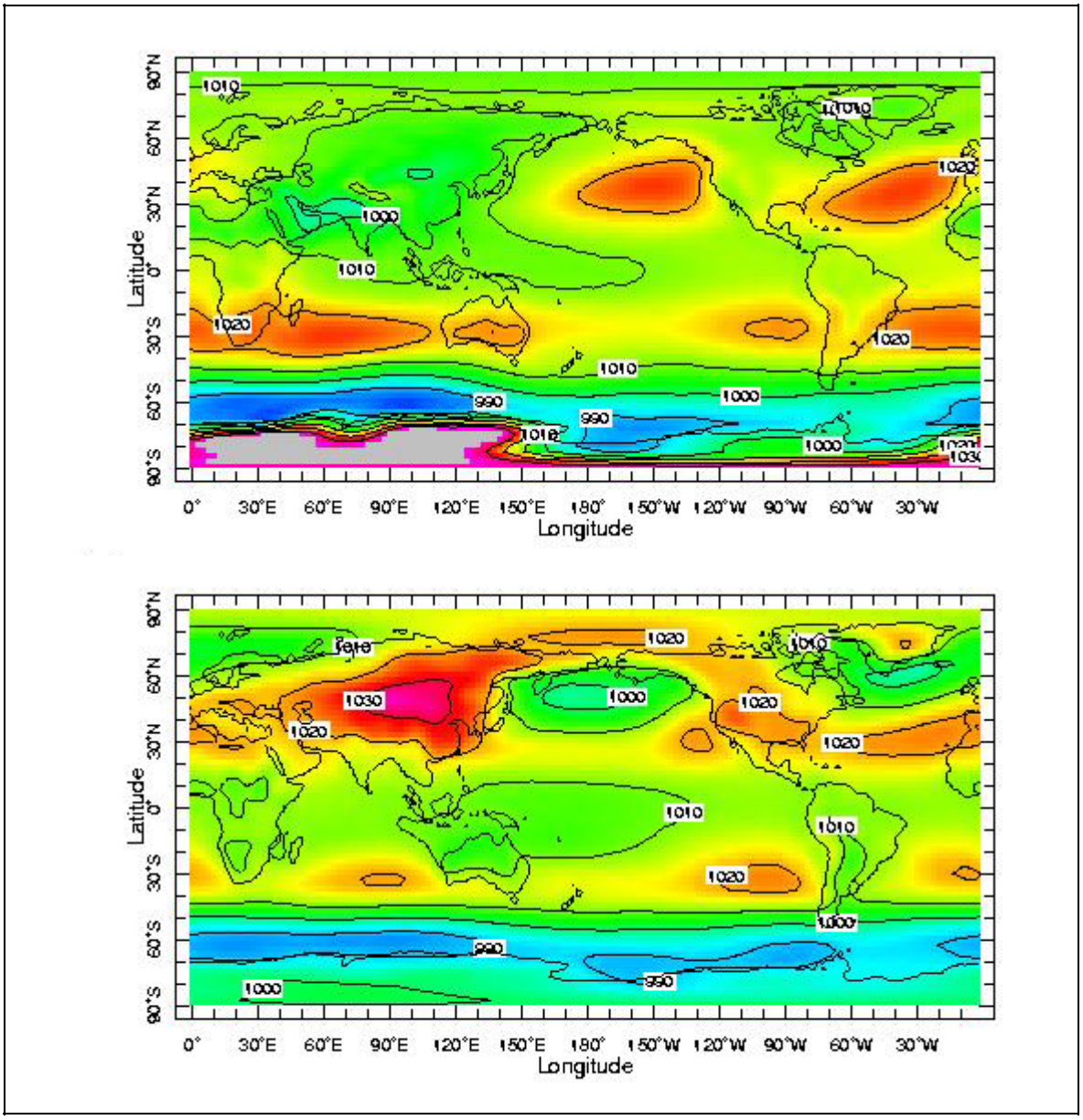

Figure 2.4. The worldwide pressure distribution for July and January, respectively

The distribution of Highs and Lows over the earth for January and July can be seen in Figure 2.4. These figures show clearly the marked difference between the pressure patterns of northern hemisphere and southern hemispheres. The large land area of the northern hemisphere causes a much more marked contrast between summer and winter conditions than in the southern hemisphere where the oceans predominate.

By looking at the figures, following conclusions appear: In winter, the equatorial belt of low pressure is located at well to the south of the equator, especially over the warm

continents of the southern hemisphere. The subtropical belt of high pressure in the southern hemisphere lies at latitudes 30-40^{o} with centers over the Pacific, Atlantic, and Indian oceans. The subtropical belt of high pressure in the northern hemisphere is located well to the north, with weak centers over the Atlantic and Pacific oceans. Relatively high pressure exists over North America and Eurasia. Deep Lows are present in the north Pacific Ocean (the Aleutian Low) and the North Atlantic Ocean (the Icelandic Low). In summer, The equatorial below-pressure belt is located well to the north of the equator, especially over the warm land areas of the northern hemisphere. The subtropical belt of high pressure in the northern hemisphere is well developed over the oceans, especially the Pacific Ocean. In the southern hemisphere, high pressure encroaches only slightly on the continents because there is so little land area in the high latitudes. Relatively low pressure exists at high latitudes in the southern hemisphere.

2.3. WIND AND GENERAL CIRCULATION

The wind is one of the most important single component of the weather. It is important in its own right as an element of the climate, but it is even more important in its influence on other components, especially temperature. Storms, clouds, rain, snow, hot spells, and sudden freezes all depend on the wind to transport the heat and moisture that cause them. However, wind is by no means independent of other components, it depends in large measure on temperature differences for it is the source of energy and these very temperature differences are often caused in part by heat gained or released in the condensation processes.

2.3.1. Forces Acting on Wind Flow

Whenever the pressure is not perfectly uniform there is a gradient of pressure. Because of the pole-equator temperature gradient, isobaric surfaces slope down from equator to pole inducing a horizontal pressure gradient at upper levels. There is thus a pressure gradient force aloft directed from high pressure to low pressure as from warm latitudes to cold latitudes (Marshall and Plumb, 2004).

Take a pressure field in which isobars delineate everywhere the value of the pressure (Figure 2.5). At point P the direction of the pressure gradient vector will be perpendicular to the isobars, and pointing toward low pressure.

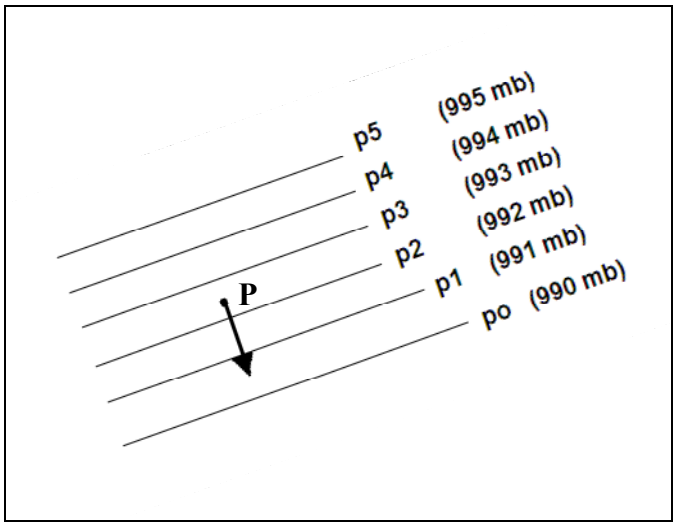

Figure 2.5. Illustration of pressure gradient

The magnitude of the pressure gradient is given in pressure decrease per unit distance. In the figure, this amounts to 2 millibars, and this is the pressure gradient at **P**. This may be expressed symbolically as *dp/dn*, or the rate of change of pressure with distance. If the air density is included in the expression, the expression will yield $(1/\rho)$ (dp/dn) which is called pressure gradient force, acts upon a unit mass of air.

As the air moves over the surface of the Earth according to pressure gradient force, the individual air particles are continuously affected by the motion of the surface as the Earth spins on its own axis. This motion of the Earth continuously deflects any freely moving object to move toward the right in the northern hemisphere and toward the left in the southern hemisphere. These deflections are the result of Coriolis force, which is formulated as:

$$F = 2mv\omega \sin\phi \tag{2.13}$$

Where m is the mass, v is magnitude of the velocity vector, for given latitude ϕ, $\omega\sin\phi$ is the component of angular velocity of the earth that is perpendicular to v.

These are the only forces acting on the winds when there is no friction. That would be a good approximation for the upper layer of the (free) atmosphere. In the case of geostrophic winds, when the wind blows in a straight line, with no acceleration or frictional forces acting on it, the only forces involved are the Coriolis end the pressure gradient forces. These are equal in magnitude and directed at right angles to the wind in opposite direction. For the latitudes above about 20° the geostrophic equation states that

$$c = \frac{1}{2\omega\sin\phi\rho}\cdot\frac{dp}{dn} \tag{2.14}$$

However, if the case is surface winds, the force of friction cannot be neglected and the forces acting on an air mass can be shown as in Figure 2.6.

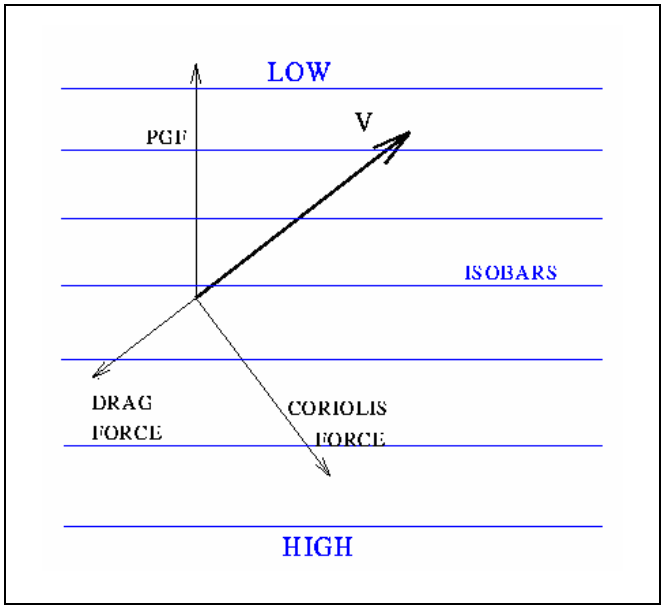

Figure 2.6. The forces acting on the wind

Friction deflects the wind so that it always has a component from high pressure to low pressure and this provides a mechanism for the interchange of air between high and low pressure systems. With local winds where the Coriolis force does not have much

effect, balance of forces may be almost entirely between pressure gradient and friction forces. Such cases may also occur near the equator where the Coriolis force vanishes. Winds of this type, where the pressure gradient force is balanced by friction, is called antitriptic winds.

As a summary, there are three main forces acting on the air masses. While force of friction always acts in the opposite direction of the velocity vector, **u,** of wind**,** pressure gradient force is applied in direction from Highs to Lows and Coriolis force always perpendicular to **u**.

2.3.2. General Atmospheric Circulation

The pole-equator temperature gradient causes an isobaric surfaces slope down from equator to pole inducing a horizontal pressure gradient at upper levels. There is thus a pressure gradient force aloft directed from high pressure to low pressure i.e. from warm latitudes to cold latitudes. Now air tends to move down the pressure gradient and so we must get a circulation. Hadley suggested one giant meridional cell with rising motion in the tropics and descending motion at the pole (Marshall and Plumb, 2004).

If the Earth was not rotating, the circulation driven by the pole-equator temperature difference would be straightforward, with warm air rising in low latitudes and cold air sinking at high latitudes as Hadley suggests. However as the Earth rotates, what Hadley suggests cannot reflect the all facts of general circulation. The consideration of mean zonal winds will be illuminating (Marshall and Plumb, 2004).

The typical distribution of mean zonal wind in the annual mean and solstices is shown in Figure 2.7. Except close to the equator, the zonal mean winds are eastward almost everywhere. The strongest winds are found at the core of the subtropical jets, the strongest of which is located near 30° latitude in the winter hemisphere and near 10km altitude (associated with the tropopause gap) with, on average, a speed of around $30ms^{-1}$. A weaker jet of about $20ms^{-1}$ is located near 45° in the summer hemisphere. The bands of easterlies observed in the tropics are much weaker, especially in northern winter. Note that

the winds are much weaker near the ground, but show the same pattern: westerlies poleward of about 30°, and easterly equatorward (Marshall and Plumb, 2004).

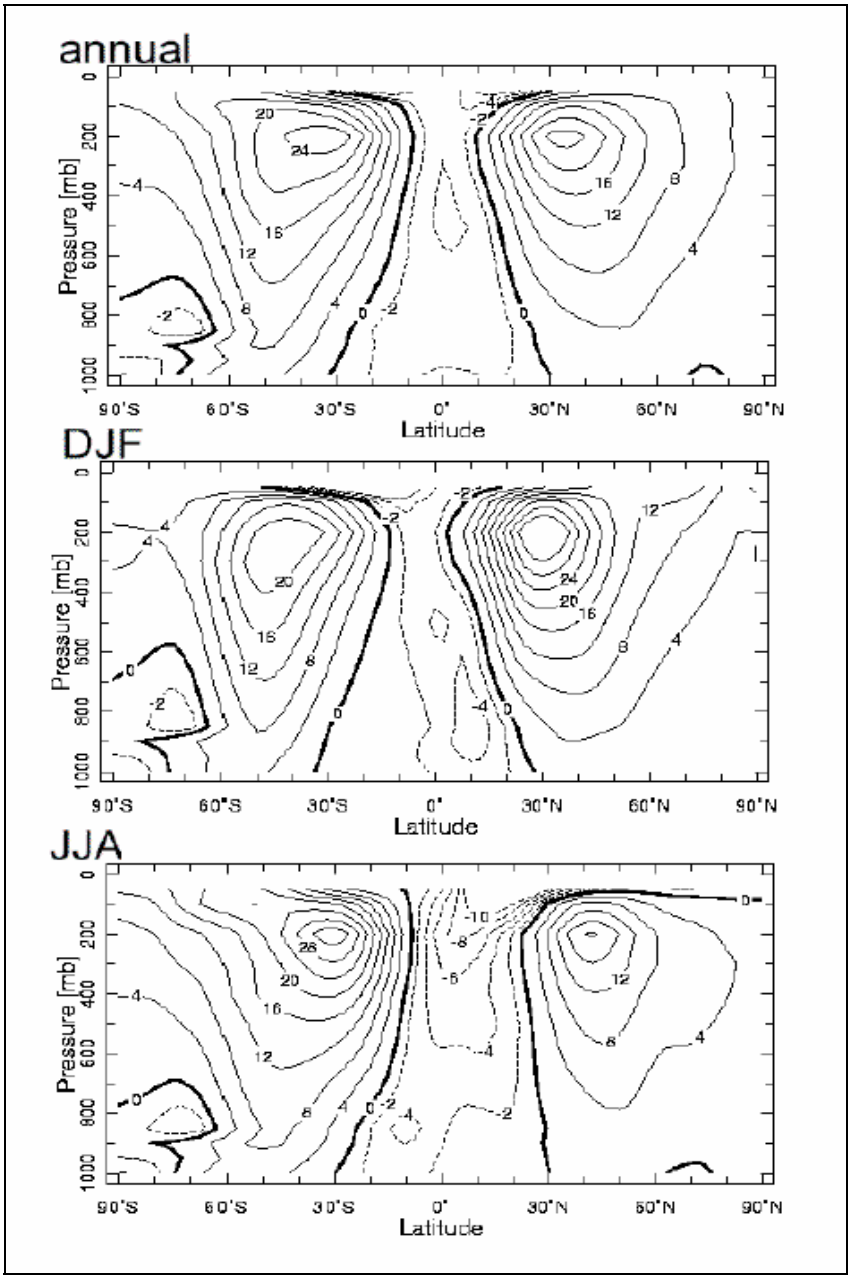

Figure 2.7. The Meridional cross-section of zonal wind (ms^{-1}) under annual mean conditions, DJF (December, January, February), and JJA (June, July, August) conditions

Figure 2.7 can be summarized as; meridional cross-section of zonal wind will under annual mean conditions shows that, indeed, a meridional circulation in the tropics with the sinking motion is located in the subtropics around latitudes of ±30°. In other words, one

giant axisymmetric meridional cell extending from equator to pole is not possible on a rapidly rotating planet such as Earth.

In order to understand this giant axisymmetric meridional cell, Figure 2.8 shows zonal mean circulation of the atmosphere in the meridional plane, is explanatory. In DJF (Dec, Jan, Feb) air rises just south of the equator and sinks in the subtropics of the northern hemisphere, around 30°N. In JJF (Jun, Jul, Aug), air rises just north of the equator and sinks in to the subtropics of the southern hemisphere. Thus, strong upward motion is seen on the summer side of the equator, where the warm ocean triggers convection and rising motion, and strong descent on the winter side of the equator. In the annual mean, two weaker cells are seen, one branching north and the other south. The overturning circulation of the tropical atmosphere evident in Figure 2.8 is known as the Hadley cell and the weaker cells in the subtropics of each hemisphere are known as Ferrel cells.

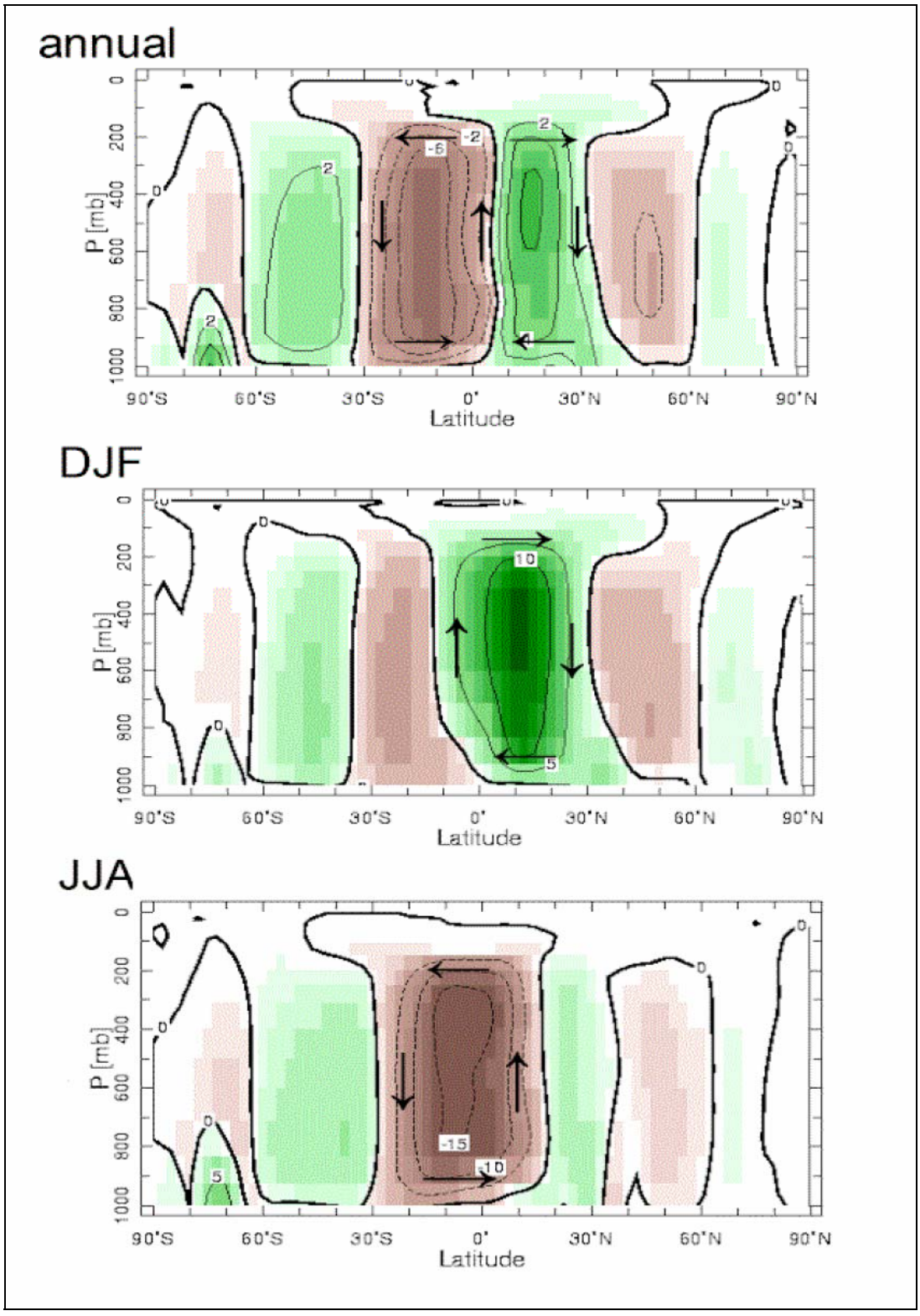

Figure 2.8. The meridional overturning streamfunction of the atmosphere in annual mean, DJF and JJA conditons. Units are in 10^{10} kgs^{-1}. Flow circulates around positive (negative) centers in a clockwise (anti-clockwise) sense. Thus, in the annual mean, air rises just north of the equator and sinks around ±30°

Consideration of the upper branch of the meridional overturning streamfunction of the atmosphere in annual mean in Figure 2.8 results the following explanations. Near the equator, where the Coriolis effect is weak, and angular momentum constraints are not so severe and the equatorial atmosphere acts as if the Earth were rotating slowly. As air moves away from the equator, however, the Coriolis parameter becomes increasingly large and, in the northern hemisphere, turns the wind to the right, resulting in a westerly component to the flow. At the poleward extent of the Hadley cell, then, it is expected to find a strong westerly flow. This subtropical jet is driven in large part by the advection from the equator of large values of absolute angular momentum by the Hadley circulation. Flow subsides on the subtropical edge of the Hadley cell, sinking in to the subtropical highs, before returning to the equator at low levels. At these low levels, the Coriolis acceleration, again turning the flow to the right in the northern hemisphere, produces the "trade winds", northeasterly in the northern hemisphere (southeasterly in the southern hemisphere). These winds are not nearly as strong as in the upper troposphere because they are moderated by friction acting on the near-surface flow. The surface winds in this axisymmetric model would be westerly at the poleward edge of the circulation cell, and eastward near the equator (Marshall and Plumb, 2004). The general circulation of the atmosphere can be subdivided as tropical circulation, the Horse Latitudes, the zone of prevailing westerlies and the zone of polar easterlies.

In general, it can be said that in the tropical latitudes (roughly from 30°N to 30°S) air from both hemispheres streams toward the equator in the two great easterly trade wind belts. In the northern hemisphere the trades blow from the north east, and in the southern hemisphere they blow from the southeast. The trades are the steadiest wind known. The trade wind system of the two hemisphere are separated near the equator by the doldrums belt. A region of convergent air flow characterized by light winds, low pressure, and strong vertical convection, with wide spread shower activity.

Somewhere around the 30° to 40° in both hemispheres, the trade winds weaken and are replaced by the subtropical high-pressure belt. This region is often called the horse latitudes. It is a region of light variable winds with little rain or cloudiness, and generally high barometric pressure. The winds in the horse latitudes are generally easterly in the lower latitudes where they merge with the trades, and westerly in the higher latitudes

where they merge with the prevailing westerlies. The high atmospheric pressure that is typical of the horse latitudes is developed clearly only over the oceans.

North of the horse latitudes in the northern hemisphere and south of them in the southern hemisphere, the great belts of prevailing westerlies take over and extend to latitude 55^0 or so. This is the region of great cyclonic storms of strong temperature contrasts, and of superhurricanes winds aloft. It is the region of the roaring forties of the southern hemisphere where steep pressure gradients maintain usually powerful and steady west winds. The zone of prevailing westerlies in each hemisphere represents the meeting ground of warm tropical air form the horse latitudes and cool Arctic air from high latitudes. During the winter season the circulation becomes intense, frequent storms occur, and the westerly belt pushes far toward the equator.

The prevailing westerlies extend to about latitude 55°. At higher latitudes, the average wind swings around and becomes easterly above about latitude 65°. This region is called the zone of polar easterlies.

2.3.3. Thermal Circulation and Local Wind Types

The basic cause of all air flow, in the atmosphere, may be found in temperature contrasts. The air over the land is heated and rises due to decrease in its density . Cool air from the ocean flows in to take place, and partially closed circulation arises. On larger scale, this happens between the ocean and entire continents in the summer. On a continental scale, this is called a monsoon circulation from its most famous type region in India.

When the ocean is cool and the land is warm, the developed sea breeze may be strong. When conditions are reversed and the land is cold relative to the water, the air flows from the cold land to the warm water. On a small scale, this produces a land breeze, often noted along coastal regions during the night. On a large scale, the flow is from the cold continents to the warm oceans in the winter.

The local winds occurs according to described dynamics above, are actually of two main types, hot and cold. Hot winds may be caused importation of hot air from a warm source region as in the case of upper level of the thermal circulations, or by dynamic heating of air as it descends from a high region to low one. Cold winds may be caused by the bringing in of cold air from a cold source region or by gravitational flow of cold air down from an elevated area to lowland area.

Highly heated air that is over the Sahara Desert moves over the southern border of the Mediterranean Sea and brings dry, searing conditions that may last for several days. The typical dynamical heated warm wind is the foehn of the Northern Alps. The forced descent of the air heats it dynamically, obeying the Equation 2.7. At the same time, the relative humidity falls quickly, so that the air reaching the plains is hot and dry.

The norther part of the Great Plains of North America is a good example of a cold wind caused by the importation of cold air from a cold source region. In the norther part, continental Arctic air from northern Canada flows rapidly southward over the Mississippi Valley, bringing tremendous and quick temperature drops (Taylor, 1954).

3. TERRAIN INDUCED WIND FIELD MODELLING

The transport of biological, or chemical hazards by the atmosphere is heavily dependent on both the mean and fluctuation (turbulent components) of the wind. There are many computational tools for predicting transportation of these hazards and most of these tools require a wind field over the entire domain, consisting of the mean wind components on a Cartesian grid, which are usually interpolated wind field or output of diagnostic or prognostic wind field models.

The interpolated wind field is created from whatever observations are available by interpolating between (or extrapolating from) those observations onto the three dimensional lattice of grid points, usually using weight factors that typically vary as the inverse square of the horizontal distance between the data and grid points. So, interpolated wind fields are generated easily and quickly, an important consideration when one is operating in the field and "real- time" predictions may be necessary.

One problem with using such an interpolated field is that in general it will not satisfy the equation representing conservation of mass, often referred to as equation of continuity. For flows over scales on the order of 10s to 100s of km, the density ρ may be reasonably assumed constant, in which case the continuity equation reduces to (Sherman, 1978):

$$\nabla \cdot \vec{u} = 0 \tag{3.1}$$

Note that this equation is already linear, with no further approximation needed. The observations themselves will invariably contain some error, and the interpolation procedure applied to them, obviously, as it is to any kinematic restrictions, will introduce further errors of its own. Hence, it would be extremely fortuitous if the interpolated wind field did not violate the Equation 3.1 by retaining a nonzero divergence at most point in the flow. A second problem with the use of interpolated winds is that they make no correction for terrain effects. The flow is as likely to go through an obstacle, such as a mountain, as it is to pass around or over it.

In an ideal world, a full (nonlinear) primitive equation model would be used to predict the wind field, including the influence of topographic changes. However, such models require considerably more computer resources as compared with a simple interpolated wind field, and may take several hours, if not days, for a complete solution.

There are two classes of three-dimensional wind field modeling that can produce fast, as appropriate for real time applications, and satisfactory results. The first consists of the so called mass consistent or diagnostic models, which use the interpolated field as input to an algorithm which makes corrections to ensure that the surface wind is parallel to the underlying terrain, and that Equation 3.1 is satisfied at each grid point as well. The second class consists of prognostic models, which solves momentum conservation equations in addition to the continuity equation. Unlike in diagnostic models, the starting point is not an interpolated wind field, rather prognostic models perform small perturbation analysis about an assumed oncoming flow. The steady-state form of the equations is solved, so that only the flow at the current instant can be studied, not its evaluation with time.

3.1. DIAGNOSTIC MODELS

As noted in the previous section, diagnostic or mass consistent models attempt to adjust the interpolated wind filed so that Equation 3.1, the continuity equation for incompressible flow, is satisfied at each grid point, and there is no through flow at the surface.

Available diagnostic models fell into four broad categories, which they termed Direct-Differencing, Point-Iterative, Hybrid and Variational Calculus (Kitada, *et al.*, 1983). Table 3.1 lists each category in a separate column, with examples of each type listed in chronological order below the appropriate heading. The chronology may not be quiet accurate but an attempt has been made to reference the latest information (Homicz, 2002).

Table 3.1. Morphology of diagnostic models

DIRECT–DIFFERENCING	POINT–ITERATIVE	HYBRID	VARIATIONAL CALCULUS
Reynolds, *et al.* (1973)	Endlich (1967); SST	Goodin, *et al.* 1980) TFC	Sasaki (1958, 1970)
Peters & Jouvanis (1979)	Liu&Goodin(1976); SST	**DIMCOR** Giarola, *et al.* (1995) SST	**MASCON** Dickerson (1978); 2D, SST
Carmichael & Peters (1980)	Endlich (1984): TFC	**CALMET** Scire, *et al.* (2000); TFC	**MATHEW** Sherman (1978) part of ARAC/LLNL; 3D ext. of MASCON; SST
Anderson (1971)	**WOCSS** Ludwig, *et al.* (1991)	**TAMOS** Pechinger, *et al.* (2001) Stohl, *et al.* (1997) TFC	**NOABL** Traci, *et al.* (1978); either SST or TFC
Liu and Yocke (1980)			**COMPLEX** Bhumralkar, *et al.* (1980) Endlich, *et al.* (1982); TFC **ATMOS1** Davis, *et al.* (1984)/LANL, TFC **MINERVE/SWIFT** Geai (1987) Sontowski, etal.(1994,1995); part of HPAC; TFC Barnard, *et al.* (1987) **NUATMOS** Ross, *et al.* (1988, 1991) ext. of ATMOS1; TFC **CONDOR**, **REDBL** Moussiopoulos, *et al.* (1986, 1988) TFC Mathur and Peters (1990) **WIND04** Venkatesan *et al.* (1996) **MEM3D** Montero, *et al.* (1998) Unstructured, FE sol'n. Harada, *et al.* (2000)

3.1.1. Direct-Differencing

Direct-Differencing approach is typically used when no information is available for the vertical component of the wind. The initial fields of the two horizontal components u_i and v_i that are assumed known throughout the domain of interest; they may result from the interpolation of available observations. Equation 3.1 may be written in Cartesian coordinates as:

$$-\frac{\partial w_i}{\partial z} = \left(\frac{\partial u_i}{\partial x} + \frac{\partial v_i}{\partial y} \right) \tag{3.2}$$

The single boundary condition required is that of no through flow at the surface, $z = h(x,y)$, which for relatively flat terrain is simply $w = 0$. Thus if the domain is overlaid with a lattice of Cartesian grid points, this equation can be approximated in terms of finite differences, and the solution for w marched upward in z. As the horizontal components are left unchanged , the mass balance at any grid point is independent of that at neighboring points. Hence no iterations are required, and one pass through the field is all that is required to enforce Equation 3.1 everywhere. The final three-dimensional wind field is given by $u = u_i$, and $v = v_i$, and w as described in Equation 3.2.

Equation 3.2 is useful primarily for flat terrain or approximately so. However, correction of the velocity field to satisfy Equation 3.1 is most important for complex terrain. The use of Equation 3.2 in such situations is problematic because the surface at which the boundary condition must be applied is now highly irregular, and no longer coincides with a constant value of one of the coordinates. However, there is one more solution is to use terrain-following coordinate:

$$\sigma = \frac{z - h(x,y)}{H(x,y,t) - h(x,y)} \tag{3.3}$$

where h is the surface height above some reference level, and H is the corresponding height of the top domain. The latter is typically placed at the top of the boundary layer, or

at the the top of the domain. The latter is typically placed at the top of the boundary layer, or at the base of an elevated temperature inversion (Reynolds *et al.*, 1973).

Terrain following coordinates are used in several mass-consistent models not just those based on Direct- Differencing (Ratto, *et al.*, 1994). Although the domain in physical (x, y, z) space is highly irregular near the surface, in computational (x, y, σ) space it is a simple rectangular parallelepiped, and the boundary condition maps to derivative of σ is 0 on the surface, $\sigma = 0$. If H is assumed to be constant, in physical space contours of constant $\sigma << 1$ will conform the underlying terrain quite closely, while becoming flat as $\sigma \rightarrow 0$. After these spatial transformations are performed, the equations get complicated but the main idea, the vertical velocity is set to whether value is required to cancel the horizontal divergence.

This category of method is simple, quick and straightforward to implement. The problem with such a simplistic approach is that it ignores the observational and interpolative errors that u_i and v_i inevitably contain, and places the entire burden of satisfying Equation 3.1 on the vertical component alone (Homicz, 2002).

Models based on Direct-Differencing approach are clearly inappropriate for stable conditions in those w are expected to be of very small magnitude. Even in stable conditions unstable conditions, unless one starts with very accurate estimates for u_i and v_i , it is quite possible to end with up with w field is unreasonably very large. The resulting winds will not go through obstacles, but they may be biased in favor of going over some that they should be going around.

3.1.2. Point-Iterative

Satisfying Equation 3.1 by point iterative approach began with Endlich who first developed the scheme for two-dimensional flow. Since the scheme was two-dimensional, this approach is applicable when the vertical component of wind velocity is zero or negligibly small.

According to Endlich, from a grid point analysis of wind components, kinematic quantities such as divergence, vorticity and deformation can be computed directly. At any grid point, the divergence is determined in the usual way as the difference between the ***u*** components at the neighboring points to the east and west, and the ***v*** components to the north and south. If an appropriate small change is made to ***u*** component at the eastward point, and a change of opposite sign in the westward point, and similarly for ***v*** to the north and south, the divergence at the point of interest can be eliminated. In order to retain the original vorticity (assuming that this is desired), the changes at each point that eliminate divergence are followed by changes to the ***v*** components east and west and to the u components north and south necessary to preserve the rotation. This method of solution is based on the two simultaneous linear partial differential equations (Endlich, 1967).

$$\frac{\partial u}{\partial x}+\frac{\partial v}{\partial y}=D(j,k) \tag{3.4a}$$

$$\frac{\partial v}{\partial x}-\frac{\partial u}{\partial y}=\zeta(j,k) \tag{3.4b}$$

where D is the divergence and ζ is relative vorticity. After specifying values for each $D(j,k)$ and $\zeta(j,k)$, the values of u and v are computed as they are satisfying these equations.

If we were to set $D(j,k) = \zeta(j,k) = 0$ over the grid, Equation 3.4 would become Cauchy Riemann system which is not of special meteorological interest. However setting $D(j,k) = 0$ and $\zeta(j,k) \neq 0$ will be a meteorological case of interest. The solution from this case is obtained as follows. At a grid point (j,k), Equation 3.4 can be written in finite difference form as ;

$$\left[u_0(j,k+1)-u_0(j,k-1)\right]/2\Delta x+\left[v_0(j-1,k)-v_0(j+1,k)\right]/2\Delta y=D_t(j,k) \tag{3.5a}$$

$$\left[v_0(j,k+1)-v_0(j,k-1)\right]/2\Delta x-\left[u_0(j-1,k)-u_0(j+1,k)\right]/2\Delta y=\zeta_t(j,k) \tag{3.5b}$$

Here the subscript t is written with D or ζ signifies the temporary value that exists at a grid point at the latest stage of iteration.

At the start of each iteration, u and v are evaluated from ζ_t. If we add the alterations that are made to u and v components, in order to eliminate the divergence. Then the Equations 3.5 will follow as;

$$\begin{aligned}\{[u_0(j,k+1)+u_{RD}(j,k)]-[u_0(j,k-1)-u_{RD}(j,k)]\}/2\Delta x \\ +\{[v_0(j,k+1)+v_{RD}(j,k)]-[v_0(j,k-1)-v_{RD}(j,k)]\}/2\Delta y \\ = D(x,y)=0\end{aligned} \tag{3.6}$$

Using Equation 3.5a, this can be written as

$$u_{RD}(j,k)/\Delta x + v_{RD}(j,k)/\Delta y + D_t(j,k) = 0 \tag{3.7}$$

If the first two terms contribute equally to the divergence, then

$$\left.\begin{aligned}u_{RD}(j,k) &= -\left(\frac{1}{2}\right)(\Delta x)[D_t(j,k)] \\ v_{RD}(j,k) &= -\left(\frac{1}{2}\right)(\Delta y)[D_t(j,k)]\end{aligned}\right\} \tag{3.8}$$

This assumption is believed to be simple conceptually but other weighting factors are possible. In Endlich's work, it is claimed that other possible weighting factors proportional to the relative contributions of u and v differences to the divergence results a little difference form those obtained using Equation 3.8.

By adopting this assumption strictly, the altered values of wind components at each grid can be written, by using a prime to denote an altered value, in terms of original values and changes from Equation 3.8 as follows,

$$\left.\begin{aligned} u'_{ND}(j,k+1) &= u_0(j,k+1) + u_{RD}(j,k) \\ u'_{ND}(j,k-1) &= u_0(j,k-1) - u_{RD}(j,k) \\ v'_{ND}(j+1,k) &= v_0(j,k+1) - v_{RD}(j,k) \\ v'_{ND}(j-1,k) &= v_0(j,k-1) + v_{RD}(j,k) \end{aligned}\right\} \tag{3.9}$$

By making these changes, the divergence at the grid point (j,k) has been reduced to zero, i.e., u_{ND} and v_{ND} are non-divergent with respect to this point. However, the altered wind components change the divergence at surrounding points from that originally calculated. Also changes that are made in eliminating divergence alter vorticity to new values slightly different from desired values. If we make additional alterations u_{RR} and v_{RR} to restore the vorticity at point (j,k) to the desired value, the equation corresponding to Equation 3.8 becomes

$$\left.\begin{aligned} u_{RR}(j,k) &= -\left(\frac{1}{2}\right)(\Delta y)\left[\zeta_t(j,k) - \zeta(j,k)\right] \\ v_{RR}(j,k) &= -\left(\frac{1}{2}\right)(\Delta x)\left[\zeta_t(j,k) - \zeta(j,k)\right] \end{aligned}\right\} \tag{3.10}$$

The components u_{RR} and v_{RR} are applied to neighboring points giving new value of u_{ND} and v_{ND}

$$\left.\begin{aligned} u''_{ND}(j-1,k) &= u'_{ND}(j-1,k) - u_{RR}(j,k) \\ u''_{ND}(j+1,k) &= u'_{ND}(j+1,k) + u_{RR}(j,k) \\ v''_{ND}(j,k+1) &= v'_{ND}(j,k+1) + v_{RR}(j,k) \\ v''_{ND}(j,k-1) &= v'_{ND}(j,k-1) - v_{RR}(j,k) \end{aligned}\right\} \tag{3.11}$$

After all these calculations are done for the point (j,k), the velocity field given by Equations 3.9 and 3.11 satisfies both D(j,k) = 0 and ζ_t(j,k) = ζ(j,k). In the same manner, entire domain is updated. All these calculations result in D(j,k) $\neq$ 0 and ζ_t(j,k) $\neq$ ζ(j,k) as well u and v values will be somewhat different from those given in Equations 3.9 and 3.11. This result shows that an iterative process is necessary. So all this procedure is applied repeatedly until the largest magnitude of D(j,k) in the domain is less than some predefined number.

The final step in the computation is to adjust the non-divergent components u_{ND} and v_{ND} so that their values averaged over the grid are equal to the averages of the original wind components. The adjustment is simply by computing the averages values of u_{ND} and u_0 and subtracting their difference from u_{ND} and similarly for the v components. In practice, the differences prior to adjustment have been found to be small, on the order of 1-2 m sec^{-1}.

Liu and Goodin (1976) claim that the procedure is explained by Endlich, while reducing the divergence, nevertheless results in wind fields that differ substantially from the original observations (Homicz, 2002). They suggest a modified scheme that is mainly based on Endlich's Point-Iterative scheme. The modified scheme differs from Endlich's in three aspects.

First of all, they define the divergence in terms partial derivatives of volumetric fluxes in horizontal directions instead of partial derivatives of horizontal velocities as Endlich did.

$$\frac{\partial(uh)}{\partial x} + \frac{\partial(vh)}{\partial y} = D \tag{3.12}$$

Liu and Goodin considered a quasi-stationary wind field where the time rate of change of the inversion base is small in relation to other spatial variations. The volumetric fluxes per unit length, uh and vh, always appear together. Determination of the wind components would require some knowledge of the inversion base height h (Liu and Goodin, 1976).

After divergence was redefined, another parameter $f_{p,q}$ is introduced, which indicates whether the grid point (p,q) is the location of a wind station. The value of f *is* zero at a station and unity at a non-station. In order to reproduce the observed data exactly with the final field, any correction had not been made at the points for which, value of f is zero.

Obviously, Endlich's formalism is not restricted to the four-point finite difference scheme and they carried out the formalism to eight-point finite difference stencil. And this

adds the new parameters to formalism. The new parameters are β and α premultiplies the average values of average values of u_{ND} and v_{ND} in Endlich's formalism and c controls the mixing of information between the four points in the Endlich's formalism and the additional four points in the eight point stencil. If the value of c is unity, only the original four points are included whereas zero value of c yields to consider only additional four points.

The last main difference between two formalisms is that in the new formalism no attempt is made to conserve vorticity, ζ. Apart from these explained modifications, the iteration procedure was same with the Endlich's.

It was shown that the modified procedure can reproduce the original observations unlike Endlich's procedure can. However, Lui and Goodin's results contain components that produce very erratic looking wind-vector plots.

The biggest disadvantage of both of these Point-Iterative schemes is their two-dimensionality. Since the vertical component of velocity is assumed to be negligible in both studies, the divergence can only be reduced by adjusting the horizontal wind components. This assumption makes these methods to be appropriate for stable or stratified conditions. Endlich continues to develop his model then Ludwig and his colleagues seek to generalize Endlich's lastly developed procedure. These later developments in Point-Iterative scheme will be discussed in the fourth chapter.

3.1.3. Hybrid

The first two approaches are convenient for the two contrast cases. The Direct-Differencing approach is based on the idea of removing non-divergence by adjusting the vertical velocity. Obviously, this approach does not hold for the stratified atmospheric conditions in which Point-Iterative schemes are very convenient. However, for the neutral or unstable conditions Point-Iterative schemes fails while the Direct-Differencing schemes work properly. Therefore, as its name suggests, a third approach was developed as a hybrid

of the first two, which attempts to satisfy continuity equation for all three wind components.

The first wind field generation algorithm of Hybrid approach was done by Goodin in 1980 (Homicz, 2002). Goodin's study consists of several basic steps. As a starting point, the region boundaries, vertical extent and basic grid cell sizes must be chosen. Once the grid has been established, the surface level velocity measurements and upper level wind and temperature data are interpolated to specify initial values for each computational point. The final step is to adjust the velocity field with the objective of minimizing anomalous divergence (Goodin *et al.*, 1980).

The surface wind field is constructed from the measured data (converted to u and v components) by interpolation to regular grid using inverse distance-squared weighting (Goodin *et al.*, 1979). The influence of gross terrain features like mountains is accounted for by use of barriers to flow during interpolation. Following the interpolation procedure, a local terrain-adjustment technique, which is similar to that of Anderson (1971, 1973), is used in the wind field calculation. This adjustment procedure involves solution of Poisson's equation.

$$\nabla^2 \phi = \Psi(x, y) \tag{3.13}$$

where Φ is a velocity potential and Ψ a forcing function based on layer thickness and terrain gradients. After an evaluation of solution techniques, based on its efficiency and accuracy considerations, the alternating-direction-implicit method, ADI method, was chosen. The ADI method was developed by Peaceman and Rachford (1955).

Thus far, only the horizontal surface winds have been defined. The approach taken for spatial interpolation of mixing depth and upper level wind data is slightly different from that used for the surface quantities. Since the measured data is not very precise, a highly accurate interpolation procedure is unnecessary. Therefore, r^{-1} weighting is chosen because, with respect to r^{-2} weighting, it produces smoother results.

Once the surface level flow field has been established and the upper level wind data have been interpolated to the three dimensional grid, the next step is to reduce the divergence in the total flow field. The divergence in each of the interpolated *u* and *v* fields at each vertical level above the lowest later is first reduced using a highly modified version of the simple five-point filter (Goodin *et al.*, 1980). This step is designed to reduce as much of the anomalous divergence as possible. Following this initial smoothing step, the vertical velocity above each layer is computed from the divergence with in that layer. The layers are temporarily disconnected from each other during this calculation so that the calculated vertical velocity above a layer depends only upon the divergence within that layer. This prevents velocities at the top of the region from becoming unrealistically large. These vertical velocities will be held fixed through out the rest of the divergence reduction procedure (Goodin *et al.*, 1980). This step can be considered as a correction to erratic part of Direct-Differencing approach on unrealistically large values of vertical component of wind velocity. The final refinement reduces the remaining divergence which exists with in each layer by application of a two dimensional technique to each layer similar to that (Liu and Goodin, 1976) has been discussed in the previous section. In this approach no attempt is made to preserve the vertical component of vorticity however, as in the Point-Iterative scheme, while the divergence is cancelled for any fixed point in the final refinement, this cancellation may cause to contaminate the divergence at the neighboring points. This is why an iterative process is needed.

Hybrid procedures such as discussed above represent a patchwork of disparate approaches, each designed in some way to compensate for the deficiencies in the others. Yet, while compensating the deficiencies, many ad hoc assumptions and approximations appear in the formulation (Homicz, 2002).

3.1.4. Variational Calculus

The starting point of the approach that will be discussed in this section mostly was developed by Sasaki who published his first studies for the application of the calculus of variations to problem of wind field modeling in 1958 and extended his own studies with other two publications in 1970 (Sasaki, 1958; 1970a, 1970b). Sherman accepted Sasaki's

studies as the theoretical basis for his model, MATHEW, and generalized the variational formalism for three dimensions. In this section, formulation of Variational Calculus approach is followed from Sherman's study (Sherman, 1978).

The general variational analysis formalism defines an integral function whose extremal solution minimizes the variance of the difference between the observed and analyzed values subject to physical constraints, which are satisfied exactly or approximately by the analyzed values. Subsidiary conditions that are to be satisfied exactly are known as strong constraints; conditions that are imposed approximately are weak constraints. A minimal solution exists when the number of strong constraints is less than the number of variables. For this model a functional is needed to minimize the variance of the difference between the adjusted values and the original values subject to the strong constraint that is the three dimensional analyzed wind field is non divergent. The specific functional used in this study is

$$E(u,v,w,\lambda)=\int_V\left[\alpha_1^2\left((u-u^0)^2+(v-v^0)^2\right)+\alpha_2^2(w-w^0)+\lambda\left(\frac{\partial u}{\partial x}+\frac{\partial v}{\partial y}+\frac{\partial w}{\partial z}\right)\right]dx\,dy\,dz \quad (3.14)$$

where x, y are the horizontal directions, z is in the vertical direction; u, v, w are the adjusted velocity components in the x, y, z respectively; u^0, v^0, w^0 are the corresponding observed (interpolated) variables; $\lambda(x,y,z)$ is the lagrange multiplier: and the values of α_i are Gauss precision moduli taken to be $\alpha_i^2 \equiv 0.5\ \sigma_i^{-2}$. (The values of α_i are observation errors and/or deviation of the observed field from the desired adjusted field.) Identical Gauss precision moduli are assumed for the horizontal directions. The integral is over the entire computational volume. The associated Euler-Lagrange equations whose solution minimizes Equation 3.14 are

$$u=u^0+\frac{1}{2\alpha_1^2}\frac{\partial\lambda}{\partial x} \quad (3.15)$$

$$v=v^0+\frac{1}{2\alpha_1^2}\frac{\partial\lambda}{\partial y} \quad (3.16)$$

$$w = w^0 + \frac{1}{2\alpha_1^2}\frac{\partial \lambda}{\partial z} \tag{3.17}$$

$$\frac{\partial u}{\partial x} + \frac{\partial v}{\partial y} + \frac{\partial w}{\partial z} = 0 \tag{3.18}$$

These equations are subject to the boundary conditions

$$\left.\begin{aligned} n_x \lambda \delta(u) = 0 \\ n_y \lambda \delta(v) = 0 \\ n_z \lambda \delta(w) = 0 \end{aligned}\right\} \tag{3.19}$$

on the x, y and z-direction boundaries where the notation δ denotes the first variation of the quantity bracketed and n_x, n_y, n_z are the outward positive unit normals of the directions x, y, z (Sherman, 1978).

The equation for λ is derived by differentiating Equations. (3.15) – (3.17) and substituting the results into Equation 3.18 giving

$$\frac{\partial^2 \lambda}{\partial x^2} + \frac{\partial^2 \lambda}{\partial x^2} + \left(\frac{\alpha_1^2}{\alpha_2^2}\right)\frac{\partial^2 \lambda}{\partial x^2} = -2\alpha_1^2\left(\frac{\partial u^0}{\partial x} + \frac{\partial v^0}{\partial y} + \frac{\partial w^0}{\partial z}\right) \tag{3.20}$$

Equation 3.20 is solved for λ with the boundary conditions of Equation 3.19, and the adjusted velocity field is calculated using Equations 3.15 – 3.17.

While the Sherman's procedure enforces mass conservation, in and of itself it does nothing to contain any explicit knowledge of the underlying terrain (Ross *et al.*, 1988). The surface winds in the interpolated field must have already been aligned parallel to the topography before the above adjustments are made. Use of the impermeable boundary condition in the previous paragraph will then assure that the wind component normal to the surface remains zero.

Kitada's "Variational Calculus Method" category has the members of which are based on the original concepts of Sasaki (1958, 1970) and their application by Sherman (1978) in developing the operational MATHEW model. Other models, which have developed from this approach, include a finite element version of MATHEW and models developed by Bhumralkar *et al.*, 1980 which aim to minimize computational costs. The later models utilize the linear characteristics of the model by combining solutions from the eigenvectors of the covariance matrix of the input wind component data (Ross *et al.*, 1988). All these models in the Variational Calculus approach has the advantage of treating all three wind components simultaneously in a unified framework as opposed to forcing any divergence to be cancelled by just one or two components as in the Direct-Differencing and Point Iterative approach, or some combination of all three, Hybrid approach. Beside the advantages, there are some ambiguities in the use of this method. How to specify values of Gauss precision moduli parameters in the model is a question mark. A following problem is how to decide specifying values of α_1 and α_2; whether their values can be independent from each other or can have a constant ratio as $\alpha = \alpha_1/\alpha_2$. Another weakness of the model is the necessity of using an iterative scheme but this weakness is not considered as a significant problem by most of the users, and reported run times on the order of few minutes are within the limits of real-time models.

3.2. PROGNOSTIC MODELS

In contrast to diagnostic models that only attempt to satisfy the continuity condition, the class of methods known as prognostic models aim to solve the steady-state momentum equation together with continuity equation. Prognostic models tend to follow a more uniform methodology than the diagnostic models do; most of the differences between them are concealed in the details.

3.2.1. Evolution of Prognostic Models

All the various models in this branch of wind modeling placed their own roots at the influential paper of Jackson and Hunt (1975). The problem studied is two-dimensional incompressible adiabatic flow over a uniformly rough surface on which an isolated low hill

is situated. Far upstream of the hill the oncoming wind is assumed horizontal, unidirectional (aligned with the x-axis), and a function of height only. The vertical component of the wind velocity set to zero. The horizontal component of wind on the x-axis is parameterized with the value of only z-axis, for any certain value of x-axis. So, the vertical velocity profile can be represented logarithmically. The hill profile is described in the form $z = hs(x/L)$, where h is height of the hill, the value of $s(x/L)$ is limited between zero and one. L is a characteristic length which is defined as the distance from the peak at which $s(x/L) = 0.5$ (Jackson and Hunt, 1975). All the parameters in the problem are stated and the following will be a brief description of the model without digressing nuances.

The underlying premise is that the flow through out the computational domain can be considered as a small perturbation about the oncoming, undisturbed flow. That is if (u,w) and (u', w') represent the total and perturbation velocity components, respectively, then

$$\left.\begin{array}{ll} u = U_0 + u' & u'/U_0 << 1 \\ w = w' & w'/U_0 << 1 \end{array}\right\} \tag{3.21}$$

This assumption allows any nonlinear terms in the equations to be replaced by ones with either constant coefficients, or coefficients whose variation with the independent variables is known a priori. However, this assumption requires some restrictions as the hill is low and of moderate slop. The analysis is strictly valid only for

$$\frac{h}{L} << 1 \tag{3.22}$$

Since the assumption of incompressible flow makes the continuity equation linear, only the momentum equations are nonlinear and require this constraint.

The energy equation is not taken into account because the flow is assumed to be adiabatic. This limits the application of the model to neutrally stable flows, or almost so. The roughness length z_0, is assumed to be constant and to satisfy

$$\frac{L}{z_0} >> 1 \tag{3.23}$$

The closure of the equations is satisfied by using a simple mixing length model. A Fourier transform is applied to the linearized equations, with respect to *x*-axis. So the original system of partial differential equations are transformed to ordinary differential equations in *z* because any differential operation with respect to *x* is replaced by an algebraic dependence on wave number, *k*. Imposing suitable boundary conditions that fix what amount to the constants of integration causes solution to be unique. To avoid imposing arbitrary boundary conditions on the transforms of velocity or pressure, the boundary layer is divided into inner region, where the turbulence is important and outer region, which is inviscid. The thickness of the inner layer is determined by balancing the competing acceleration and stress gradient terms in the inner layer. The solution should satisfy the no-slip condition as the value of *z* approaches to zero in the inner region and in the outer region the solution must be approach to freestream conditions as the value of z is going to infinity. Then by performing an inverse Fourier transform, all the perturbation fields can be transformed to spatial space and adding these values to undisturbed flow, analytical results are obtained across the entire boundary layer (Jackson and Hunt, 1975).

Later investigations extended the Jackson and Hunt (1975) model in several respects. Mason and Sykes (1979) expanded the applicability Mason and Sykes (1979) expanded the applicability of the Jackson and Hunt model by generalizing it from two to three dimensions. The principal difference is to perform Fourier transform/inverse operations with respect to both *x* and *y*, whereas Jackson and Hunt applied these transformations only in the *x*-axis. The authors highlight the qualitative nature of the differences between the two- and three-dimensional solutions, and compare the latter against experimental data obtained from Brent Knoll. The Mason and Sykes model was also programmed independently and subjected to further validation study by Taylor and Walmsley (1981). The problem with applying either the two-dimensional Jackson and Hunt (1975) or three dimensional Mason and Sykes (1979) theories to real applications is that they assume an isolated disturbance, surrounded by a uniform plain extending to infinity (Mason and Sykes, 1979).

The first investigation that attempted to apply linear theory to "real world" terrain of finite extent was that of Walmsley, *et al.* (1982). They used essentially the Mason and Sykes analysis, but with the region of interest, L_R, surrounded by a flat plain of uniform roughness, which is smaller than L. This pattern is assumed to repeat itself periodically in both x and y. The ratio L to the region of interest is set sufficiently large that periodic lateral boundary conditions can be imposed without unduly influencing the flow within the region of interest. However, if the terrain at the edges of the inner region were to change abruptly from its actual elevation to that of the surrounding plain, spurious high-frequency oscillations would result in the solution. For this reason, a transition zone is inserted between the real terrain and the surrounding plain, within which the elevation is allowed to blend smoothly between the two. This introduces an additional parameter, the ratio L_T/L_R. Finally, Walmsley, *et al.* (1982) use discrete Fourier series to transform the partial differential equations to ordinary differential equations, rather than infinite Fourier transforms, as the former are more appropriate to periodic, as opposed to isolated, disturbances.

Mason and King (1985) independently developed similar refinements to the linear theory, notably the use of uniformly valid solutions and distinct velocity scales appropriate to the inner and outer layers. They also go into somewhat more detail regarding the sizes chosen for the overall domain and the transition zone relative to the region of interest. Results showed improved agreement with nonlinear finite-difference calculations, and trends similar to those seen by Taylor, *et al.* (1983).

The above studies were all for neutrally stable flows. Hunt, *et al.* (1984, 1988a, 1988b) also continued with the development of linearized theories, notably considering the effects of various degrees of stratification and different oncoming flows. They retain the concept of inner and outer regions, but further refine the model as follows. The outer region is subdivided into an upper and a middle layer, while the inner region is subdivided into a shearstress layer and an inner surface layer (Hunt, *et al.* (1984, 1988b)). Analyses are presented for stably stratified flows assuming a logarithmic oncoming profile (Hunt *et al.*, 1988a), and for neutrally stable flows in which the oncoming flow is allowed to have either a logarithmic, power-law, or linear profile with height (Hunt *et al.*, 1988b). Belcher, *et al.* (1990) considered the effects of (one-dimensional) changes in surface roughness on

the flow, in the context of a two-dimensional flow model. Walmsley, *et al.* (1986) extended the analysis of Taylor, *et al.* (1983) to include two-dimensional variations in surface roughness in a three-dimensional flow model, again assuming neutral stratification. This incarnation is designated MS3DJH/3R. Carruthers, *et al.* (1988) employed a model that divides the turbulent boundary layer into three sub-layers: the inner, middle, and upper layers. Drawing on the ideas put forth in several earlier investigations, their model, dubbed FLOWSTAR I, incorporates the effects of various stratifications, oncoming wind profiles, and changes in both surface elevation and surface roughness. Later improvements were added, resulting in the FLOWSTAR III model (Finardi, *et al.*(1993)).

Researchers at the Ris National Laboratory in Denmark have also been active in this branch of wind modeling. Astrup, *et al.* (1997) describe their independent development of a linear model that is capable of treating inhomogeneous surface roughness. Their model is incorporated as part of the LINCOM code, which is also capable of predicting the effects of surface elevation changes and thermal stratification. LINCOM is part of a preprocessor chain known as MET-RODOS, which provides meteorological inputs to a yet larger collection of codes, RODOS (Real Time On Line Decision Support), assembled to calculate the atmospheric transport and dispersion of radioactive materials (Mikkelsen, *et al.*1997, and Astrup, *et al.*, 2001). In the evolution of Prognostic Models, one study is outstanding in the regard of making attempt to satisfy energy conservation. Troen and de Bass' (1986) model for three-dimensional model for three-dimensional neutrally stable flow is the basis on which LINCOM computes the effects of topographic variations, according to Astrup, *et al.*, 1997. However, Troen and de Baas take the linearized analysis a step further in what they term the "generalized" model. The set of equations on which this model is based includes both the energy equation and Coriolis terms (Homicz, 2002).

3.2.2. Conclusions on Prognostic Models

There is no way to guarantee a priori that the results of a linear model will in fact satisfy Equation 3.21, but certainly a necessary (though perhaps not sufficient) condition is that the terrain be gently sloping, as reflected in Equation 3.22. It is stated that h/L less than 0.05 should be sufficient to justify linearization for most purposes (Jackson and Hunt,

1975). Assuming a typical slope angle has a tangent of $h/(2L)$, this implies inclinations of no more than 2°. Yet it has been noted by several authors that such models are applied to terrain whose slopes lay outside the range of validity. Some studies show that good agreement with observations of flow speedup over hills with larger slopes than 25° (Mason and King, 1975 and Carruthers, *et al.*, 1988). In any event, linear models are clearly inappropriate for use in mountainous regions, or wherever local features such as bluffs violate these assumptions.

In prognostic models, it is assumed that each change in any of the mechanisms, surface elevation, roughness, and stratification, acts independently of the others. That is, the effects of elevation changes are computed assuming uniform roughness and neutral stratification, while the effects of roughness changes are calculated for a level plain and neutral stratification, and so on. Then because the underlying equations are linear, a composite flow field incorporating the effects of all the mechanisms is obtained by superposing the separate solutions. As a result, all the non-linear relations between the mechanisms have been neglected. Besides the numerous approximations and vague choices of physical parameter values, as h and L, there is also an unclear definition of the transition zone and uniform plain. How to decide the values of these parameters are haze.

As a conclusion, prognostic models are appropriate for relatively smaller and detailed domains. These models are appropriate to studies such as, predicting maximum wind loads on structures or evaluating alternative sites for wind tribunes.

4. WINDS ON CRITICAL DIVIDING STREAMLINE SURFACES

The winds on critical dividing streamline surfaces (WOCSS) analysis scheme was developed to produce high-resolution three-dimensional gridded wind analyses in areas of complex terrain. WOCSS belongs to that class of models that use the principle of mass conservation to compute gridded winds, given as input surface wind observations and wind and temperature soundings.

The Objective Analysis described here was to provide fast objective wind analyses in complex terrain by incorporating important physical constraints. What is described solves differential equations but preliminarily it invokes important physical principles in the adjustment of interpolated values.

Winds On Critical Streamline Surfaces incorporates conservation of mass and critical dividing streamline concept as physical constraints on the system. Simple interpolation techniques do well if the terrain is flat and the atmosphere is well mixed but it is important to generate wind fields above complex terrain when the atmosphere is stably stratified. The cooler air parcel stands on the warmer one and it prevents the warmer one from rising so a temperature inversion occurs and atmosphere is stratified (Ludwig *et al.*, 1991).

4.1. EVOLUTION OF WOCSS

Evolution of WOCSS methodology begins with wind energy planning model, COMPLEX, of Bhumralkar (1980) in which Bhumralkar used a variational calculus numerical scheme similar to Sherman's (1978) but applied it in sigma coordinates rather than Cartesian coordinates. Later Endlich (1984) replaced the variational calculus numerical scheme with iterative technique which Endlich (1967) developed earlier in order to avoid divergence.

Endlich proved that to simulate the effects of terrain on the flow is difficult by using sigma surfaces that never intersect the terrain, even in a stably stratified atmosphere.

Therefore, he lets the flow surfaces intersect the terrain and set the velocity of intersection points (subterranean points) to zero so that the nondivergence constraint would force the flow to pass around the intersected obstacles (Endlich, 1984).

The concept of critical dividing streamline was studied by Sheppard (1956) and Hunt and Synder (1980). The principle underlying the critical dividing streamline concept is that there is some height where the work done against buoyant restoring force (as the air is displaced from its equilibrium position), equals the original kinetic energy of the wind. Ludwig *et al.* (1991) combined the concept of critical dividing streamline with the studies of Bhumralkar (1980) and Endlich (1984) above and produced the WOCSS code.

4.1.1. COMPLEX

The COMPLEX model is a modified version of a model which was developed by Sherman (1978), explained in the Section 2.1.4. It adjusts a three dimensional array of winds that has been derived from observations at a limited number of scattered locations by interpolating them to a horizontal grid and extrapolating them in the vertical. The adjustment processes involves minimizing the mean square difference and is constrained so that the equation of continuity of mass of an incompressible fluid is satisfied.

The COMPLEX model uses "sigma" (σ) instead of the vertical component of z as the vertical coordinate; σ is defined as

$$\sigma \equiv \frac{z - h(x,y)}{H(x,y) - h(x,y)} \tag{4.1}$$

where $h(x,y)$ is the height of the terrain above a certain reference level and $H(x,y)$ is the corresponding height of the top of the model. The surfaces $H(x,y)$ and $h(x,y)$ are assumed to be rigid impermeable boundaries.

Since σ is constant at $z = h$ and $z = H$, $\sigma = 0$ and $\sigma = 1$ respectively, the time derivative of σ is equal to zero at these boundaries. The derivative of σ with respect to time is the vertical velocity in a σ coordinate system and is related to w by

$$\dot{\sigma}(H-h) - \dot{h}(\sigma - 1) + \sigma\dot{H} = \dot{z} = w \tag{4.2}$$

The simplicity of the Equations 4.1 and 4.2 makes it possible to formulate lower and upper boundary conditions easily for complex terrains and boundary layers. So the Equations 3.15 – 3.18 can be rewritten as

$$\frac{\partial u^*}{\partial x} + \frac{\partial v^*}{\partial y} + \frac{\partial w^*}{\partial \sigma} = 0 \tag{4.3}$$

$$2W_H(u^* - u_0^*) - \frac{\partial \lambda}{\partial x} = 0 \tag{4.4}$$

$$2W_H(v^* - v_0^*) - \frac{\partial \lambda}{\partial y} = 0 \tag{4.5}$$

$$2W_V(w^* - w_0^*) - \frac{\partial \lambda}{\partial \sigma} = 0 \tag{4.6}$$

where

$$\begin{aligned} u^* &= u(H-h) \\ v^* &= v(H-h) \\ w^* &= \dot{\sigma}(H-h) \end{aligned} \tag{4.7}$$

The quantities W_H W_V are the weights assigned to the modified horizontal (u^* and v^*) and vertical (w^*) wind components, respectively; they are determined from numerical experiments.

Equation 4.3 imposes mass conservation on the adjustment process and the difference between the observed and the adjusted values of u^*, v^* and w^* is minimized on the basis of Equations 4.4 – 4.6. By eliminating different combinations of u^*, v^* and w^*, and λ from Equations 4.3 – 4.6 the following equations are obtained

$$\frac{\partial^2 u^*}{\partial x^2}+\frac{\partial^2 u^*}{\partial y^2}+\frac{W_H}{W_V}\left(\frac{\partial^2 u^*}{\partial \sigma^2}\right)=\frac{\partial^2 u_0^*}{\partial y^2}+\frac{W_H}{W_V}\left(\frac{\partial^2 u_0^*}{\partial \sigma^2}\right)-\frac{\partial}{\partial x}\left(\frac{\partial v^*}{\partial y}+\frac{\partial w_0^*}{\partial \sigma}\right) \tag{4.8}$$

$$\frac{\partial^2 v^*}{\partial x^2}+\frac{\partial^2 v^*}{\partial y^2}+\frac{W_H}{W_V}\left(\frac{\partial^2 v^*}{\partial \sigma^2}\right)=\frac{\partial^2 v_0^*}{\partial x^2}+\frac{W_H}{W_V}\left(\frac{\partial^2 v_0^*}{\partial \sigma^2}\right)-\frac{\partial}{\partial y}\left(\frac{\partial u_0^*}{\partial x}+\frac{\partial w_0^*}{\partial \sigma}\right) \tag{4.9}$$

$$\frac{\partial^2 w^*}{\partial x^2}+\frac{\partial^2 w^*}{\partial y^2}+\frac{W_H}{W_V}\left(\frac{\partial^2 w^*}{\partial \sigma^2}\right)=\frac{W_H}{W_V}\frac{\partial}{\partial \sigma}\left(\frac{\partial u_0^*}{\partial x}+\frac{\partial v_0^*}{\partial y}\right)+\frac{\partial^2 w_0^*}{\partial x^2}+\frac{\partial^2 w_0^*}{\partial y^2} \tag{4.10}$$

The wind at a given station can be obtained by integrating, independently, the finite-difference form of Equations 4.8 – 4.9. The final solution is in the form of horizontal and vertical components of wind at various levels in the vertical that have been adjusted for the underlying terrain effect and to satisfy the mass conservation principle.

The vertical distribution of wind on three-dimensional grid can be estimated by using a power law formulation of the form

$$\frac{V_2}{V_1}=\left(\frac{Z_2}{Z_1}\right)^{\alpha} \tag{4.11}$$

where V_2 and V_1 are wind speeds at the heights Z_2 and Z_1 respectively, and α is a dimensionless exponent. The value of α depends on atmospheric stability, wind speed, and surface roughness.

As a summary, wind and topographic data in gridded form are input as boundary conditions for solving Equations 4.8 – 4.10. Firstly, Equation 4.10 is solved to calculate

adjusted value of vertical velocity. Then the solutions of Equations 4.8 and 4.9 give the adjusted value of horizontal wind components. As a last step, u, v and $\dot{\sigma}$ are obtained from Equations 4.7 and Equation 4.2 is solved for vertical component of wind velocity in Cartesian coordinate, w. The resulting solution provides three dimensional grid point values of wind that explicitly incorporate the effects of topographic features.

4.1.2. Concept of Critical Dividing Streamline

The concept of critical dividing streamline applies when potential temperature increases with height, $d\theta_v/dz > 0$, and atmospheric conditions are approximately adiabatic. The principle underlying the critical dividing streamline concept is that there is some height where the work done against the buoyant restoring force equals the kinetic energy of the wind (Ludwig *et al.*, 1991).

Sheppard (1956) postulated that along a streamline kinetic energy is converted to potential energy as fluid parcels rise over the hill so the maximum amount of vertical lifting undergone by fluid parcels that travel over the mountaintop can be iteratively determined from

$$\frac{1}{2}U_{\infty}^{2}(z_t) = \int_{z_t}^{h}(h-z)N^{2}(z)\,dz \tag{4.12}$$

where $N^2 = (g/T_v)(\partial\theta_v/\partial z)$ is the Brunt-Vaisala frequency squared, $T_v(z)$ is the virtual temperature, $\theta_v(z)$ is the virtual potential temperature, and z_t is the height of the dividing streamline, the lowest initial height of air parcels that travel over the mountaintop. In the case of constant $U_\infty(z)$ and constant $N(z)$ the equation simplifies to $z_t = h(1\text{-}U_\infty/N_h)$ (Sheppard's formula). Thus the air that reaches the mountaintop has been lifted by $h - z_t = U_\infty/N$. In the following Equation 4.12 will be referred as Sheppard's model, while the term "Sheppard's formula" will refer to the simplified expression. The following assumptions underlie Equation 4.12. First, Sheppard (1956) assumed that the flow is inviscid, and that the velocity and pressure fluctuation at the summit of the hill are zero, in other words, the kinetic energy upstream has been completely converted to potential

energy when the fluid parcel reaches the summit. Ding and Street (2003) demonstrated that for inviscid flow Sheppard's formula is successful, because "the energy provided by pressure field roughly offsets the energy loss due to either friction or turbulence for axisymmetric hills.".

Second, the rotation of the Earth, and therefore the Coriolis force is neglected. This limits the applicability of the analysis to small-scale mountains or large Rossby numbers $R_0 = U_\infty/fL$, where L is the mountain half width and f is the Coriolis parameter. However, it is suggested that the Coriolis force can be only neglected for mountain widths are less than 50 km (Smith, 1980).

Third, the influence of the shape of the mountain is neglected. Shape and slope of the mountain are of importance. For example, with a slope of one only negligible lifting occurs, while surfaces with a slope between zero and one cause various amounts of lifting. Most experimental work has focused on Gaussian hills, for which Equation 4.12 has been shown to be in good agreement with observations (Hunt and Snyder 1980).

In the WOCSS approach, the Sheppard's formula is used to define critical dividing stream surfaces. Sheppard's model integrated through z_0 to Z_{max} for constant velocity $U_\infty(z)$ at the lowest altitude on the flow surface that is equal to V_0 and constant virtual temperature, $\overline{T}$, is defined as the average temperature between Z_{max} and z_0. So to determine the height of the critical dividing streamline following equation is obtained

$$Z_{\max} - z_0 = V_0 \left(\frac{d\theta}{dz} \frac{g}{\overline{T}} \right)^{-1/2} \tag{4.13}$$

4.2. WOCSS

The WOCSS analysis scheme uses the critical dividing streamline concept to restrict vertical motion under stable conditions. The critical streamline concept limits the vertical rise of the flow to that height where the potential energy gained by displacement against a stable thermal stratification equals the kinetic energy of the flow at its original altitude.

The WOCSS model also imposes mass conservation as a nondivergence constraint to force flow interaction with the terrain.

Equation 4.13 provides the basis of an objective method for defining coordinate surfaces like Endlich's (1984) subjectively defined flow surfaces. These coordinate surfaces will approximate the shape of the flow and will intersect the terrain in areas where the flow cannot pass over it (Ludwig *et al.*, 1991).

First of all, the height of the top of the domain should be defined. The top of the domain at a particular grid point is denoted by H_{top}. The average thickness of the boundary layer in the area of interest is denoted by H_a; h is the terrain height at the point of interest; h_s is the terrain height at the site; and k is the slope factor: if k is equal to one, the top parallels the terrain; if k is equal to zero, the boundary layer top is flat; the values in this range give intermediate slope. Then the basic equation is (Endlich *et al.*, 1982):

$$H = H_a + kh + (1-k)h_s \tag{4.14}$$

In order to define the coordinate surfaces first the highest and lowest terrain points in the domain are identified. Then the flow surfaces above the lowest terrain point is specified, and the model generates a corresponding set of terrain-following surfaces. After terrain-following surfaces are generated, first guess winds and potential temperature lapse rates are interpolated to those terrain-following surfaces. Interpolated winds and lapse rates over the lowest terrain point are used to determine the highest elevation $(z_{max})_i$ to which the *i*th flow surface can rise above the terrain. The derived expression from Equation 4.13, for stable lapse rate, is

$$(z_{\max})_i = (z_{\min})_i + V_0\left(\frac{d\theta}{dz}\frac{g}{\overline{T}}\right)^{-1/2} \tag{4.15}$$

and, for neutral or unstable lapse rate, is

$$(z_{\max})_i = (z_{\min})_i + (\Delta H)_{\max} \tag{4.16}$$

where $(z_{\min})_i$ is the height, of the *i*th surface above the lowest terrain point; $(\Delta H)_{\max}$ is the difference in elevation between the highest and the lowest terrain points (Bridger *et al.*, 1994). If the atmosphere were always uniformly stratified the above relationships would be sufficient to define a set of surfaces that are parallel one another, all rising by the same amount over the higher terrain. However, the real atmosphere is frequently characterized by stable layers that have neutral or unstable layers above or below them. Therefore, it is necessary to impose additional constraints on the heights to which the flow is allowed to rise. The maximum elevations for the flow surfaces are constrained such that

$$\left[(z_{\max})_{i+1} - (z_{\max})_i\right] \le 0.5\left[(z_{\max})_{i+1} - (z_{\max})_i\right] \tag{4.17}$$

$$\left[(z_{\max})_{i+1} - (z_{\max})_i\right] \le \left[(z_{\max})_{i+1} - (z_{\max})_{i-1}\right] \tag{4.18}$$

The Equation 4.17 imposes the condition that prevents the lower surfaces from penetrating or approaching too closely to higher surfaces, while the later condition keeps terrain influences from penetrating elevated stable layers. After the maximum heights to which the air can reach have been defined for each flow surface that information is used to define the flow surface heights z_i above each grid point. Here it is assumed that the extreme elevations of the critical streamline surfaces are found over the lowest and highest terrain points ($H_{\min}$ and $H_{\max}$, respectively) and that the following proportionality relationships holds over other locations:

$$z_i = (z_{\min})_i + \frac{H - H_{\min}}{(\Delta H)_{\max}}\left[(z_{\max})_i - (z_{\min})_i\right] \tag{4.19}$$

where H is the terrain height. So that, all the flow surfaces have been defined. The use of these surfaces not only incorporates the critical dividing streamline concept but also reduce the three-dimensional problem to several, more easily solved two-dimensional problem.

With the intention of obtaining adjusted wind fields, the observed winds are interpolated to produce an “initial guess”. Mass-conserving wind interpolation scheme begin with an “initial guess” and adjust it to remove the divergence. The adjustments can use either rectangular coordinates or curvilinear coordinates. The WOCSS code uses curvilinear coordinates and assumes that there is no flow through those surfaces. These flow surfaces are defined as described in the preceding paragraph. Wherever flow surfaces intersect the terrain, the wind will be zero so that mass conservation adjustments will force the flow around the intercepted obstacle.

The separation of the flow surfaces varies from place to place, therefore, mass fluxes (not the horizontal wind components, ***u*** and ***v***) must be adjusted toward non divergence. Endlich *et al.* (1982) replaced the wind component variables with flux-related variables very similar to Bhumralkar *et al.* (1980) did in the wind energy planning model. Then flux related variables are formulated as

$$\begin{aligned} u' &= u\Delta z \\ v' &= v\Delta z \end{aligned} \tag{4.20}$$

where Δz is the average separation between the surface and the two adjacent flow surfaces. At the bottom and top of the domain, Δz is the half distance to the one adjacent flow surface. If the slopes of the flow surfaces are not overly large, the continuity equation is approximated by (Ludwig *et al.*, 1991)

$$\frac{\partial u'}{\partial x} + \frac{\partial v'}{\partial y} = 0 \tag{4.21}$$

The iterative scheme described by Endlich (1967), which is explained with all details in Section 2.1.2., is used to adjust the wind estimate to satisfy Equation 4.21. So that WOCSS model iteratively adjusts the flow on each surface toward two-dimensional (with in the critical streamline surfaces) nondivergence.

5. EVALUATION OF THE WOCSS WIND ANALYSIS SCHEME FOR ISTANBUL BOSPHORUS AREA

The explained WOCSS wind analyses scheme in the preceding chapter is used for Istanbul Bosphorus area. The complex geography of Bosphorus makes the evaluation challenging. Besides, the limited number of available observation sites seems to be problematic.

With the purpose of understanding whether the limited number of sites will cause a problem or not; a literature review was done and the performance of the WOCSS for a certain dataset that had been send with its outputs by Prof. Dr. Ludwig (one of the originator of the WOCSS), was evaluated by running the WOCCS for different datasets, which were obtained by choosing fewer number of data from available ones in the dataset.

5.1. PERFORMANCE EVALUATION OF WOCSS

There are several applications of the WOCSS in literature. In these applications, the necessary data set, as an input for WOCSS code, is obtained from many different stations that can reflect the effect of topography. Especially, one study that was accomplished by Ludwig and Sinton in 1998 was done with an uncommonly comprehensive dataset.

One of the earliest applications of the WOCCS is The Southern California Air Quality Study (SCAQS) was conducted by a consortium of public and private organizations. In this study, sizes of the area of interest were 100 km in south-north and 180 km in west-east directions. There were 69 observation sites in the domain which means that on the average one observation site is available for every, almost, 250 km^2 (Ludwig *et al.*, 1991) Another study of the first applications of the WOCSS that was performed by Thykier-Nielsen *et al.*, in 1990 was a dispersion-model evaluation. The Vandenberg AFB terrain and meteorological data have been performed. The intent of this work has been to evaluate the real time dispersion model RIMPUFF driven by two alternative flow models, LINCOM and WOCSS, using the Mountain Iron data from

diffusion experiments in the hilly coastal terrain at Vandenberg AFB, California. Later, WOCSS had been applied to different areas of interest, but one of these later studies was outstanding. The October 2000 Vertical Transport and Mixing eXperiment (VTMX) in the Salt Lake Basin involved more than a dozen different organizations, collecting data with many different kinds of meteorological instruments.

In this study, the areas of interest are Bosphorus and Yeşilköy Atatürk Airport so the domain has been chosen as including these areas. With only one radiosonde data there are four observation sites that can provide data for surface meteorological measurements as wind speed and direction, temperature and pressure in the domain but the locations of the sites are representative. The available data are much less, than the ones studied in the VTMX. However, another study which was carried out by Ludwig and Sinton in 2000, showed that, although with the increasing number of available data the performance of the WOCSS increases, it is possible to have satisfactory results even with seven station input datasets out of forty available different ones with at least one upper air observation data in a domain is covered 108 × 123 grids with 1 km grids spacing. The WOCSS was applied to this domain for three different cases those were consisted of four, seven and eleven datasets of dissimilar observation sites and the results illustrated slight differences in favor of estimation of wind speed and direction for the cases.

The dataset that was send by Prof. Dr. Ludwig was taken out from VTMX datasets. In the dataset, there were 186 surface and ten (six sounding and four temperature dataset) upper air observations. The number of observations is much larger than observations that are available for our study. Then it is decided to rerun the WOCSS code for several distinct input data that will be extracted from the sample data set.

The output of sample dataset was already given by Prof. Ludwig, the output was calculated for a given 80 × 80 gridded domain with 1 km grid size. The following figures illustrate the original output of sample dataset and the area of interest.

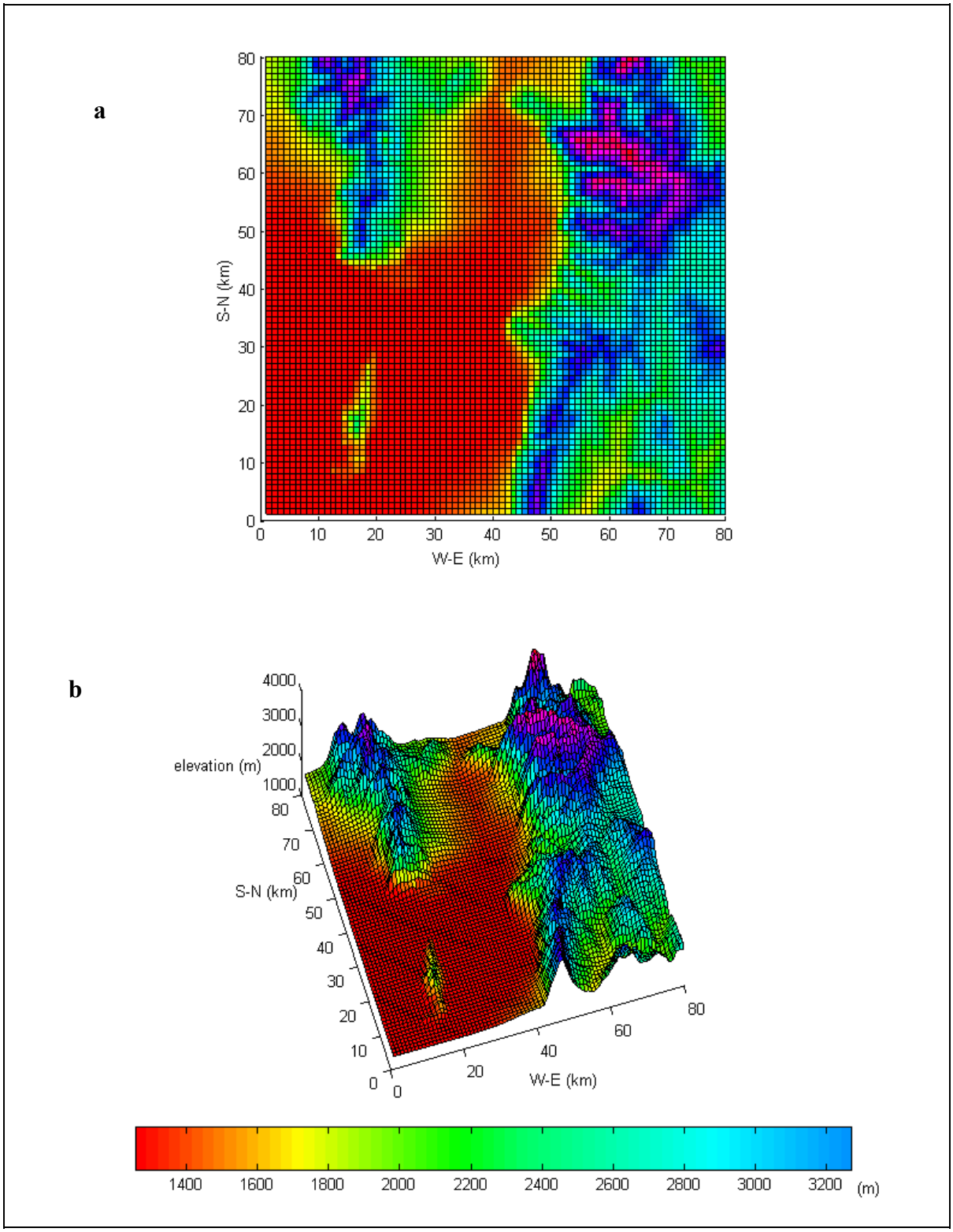

Figure 5.1. (a) Two and (b) Three -dimensional elevation model of Salt Lake domain

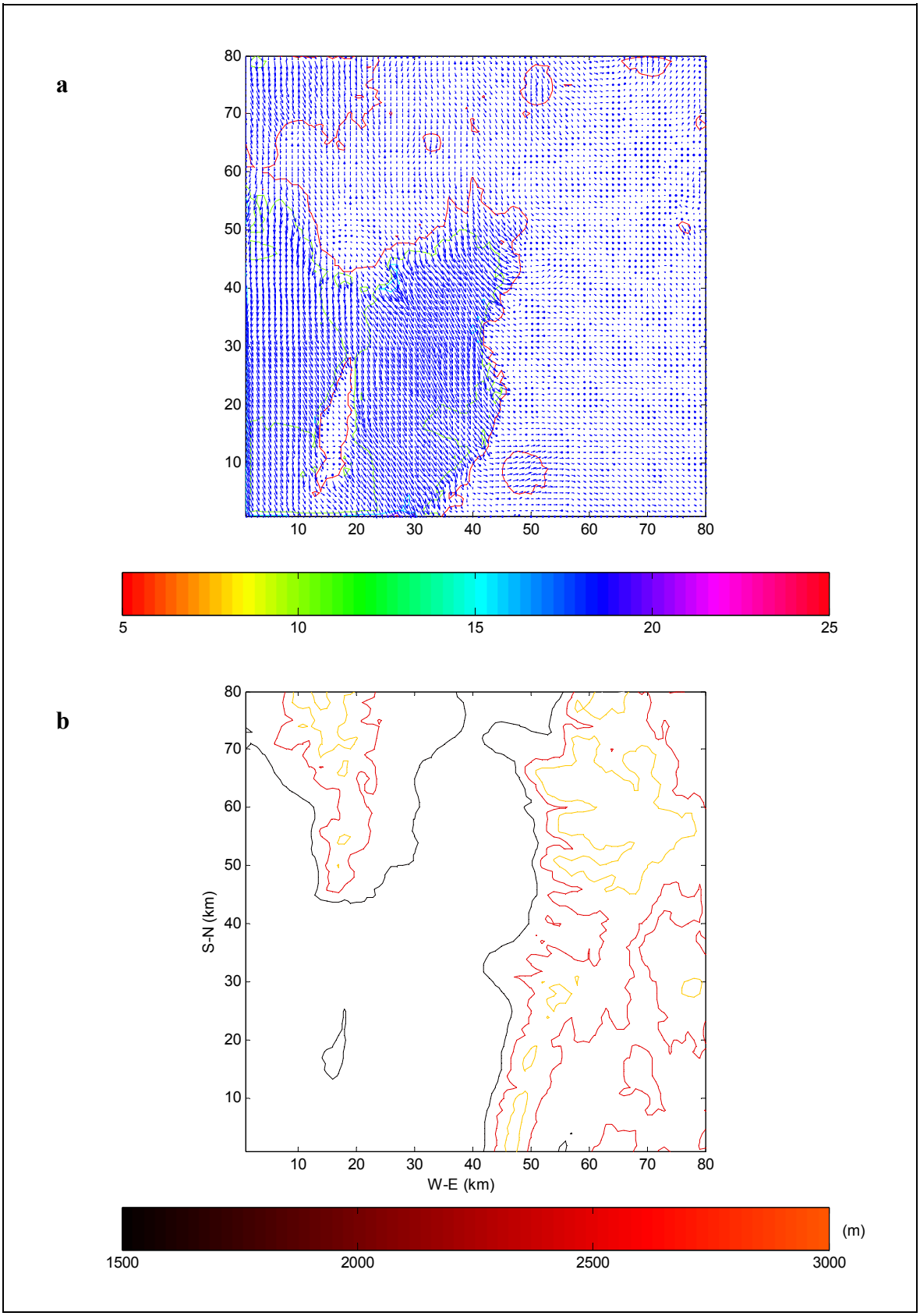

Figure 5.2. (a) WOCSS surface wind analyses of sample data at 10m above the terrain with contour representing equal speed values (b) Contour plot representation of the domain

The results of surface wind velocities that have been plotted as Figure 5.2 (a), have been obtained by log-linearly interpolation between the surface roughness height and the lowest flow surface (Ludwig *et al.*, 1991). However, these wind results were not adjusted with the constraint of mass-conservation, which is applied to upper flow surfaces. Therefore, keeping in mind that for the upper most level flow surfaces, the effect of terrain will reduce; second and other lower flow surfaces should be compared with the purpose of understanding whether the reduction of data affects the results greatly or does not. The given output of the sample data was obtained for nine different flow levels with the first one was the interpolated surface winds and the ninth flow level was the most upper one .

For comparison, the second, the forth and the eighth flow levels were chosen from the output of sample dataset. The first flow level was chosen to be at the heights of 10 above the terrain surface and the rest, beginning with the second flow level up to ninth one, were assigned to the heights 1400, 1500, 1600, 1700, 1800, 1900, 200 and 2500 m. The same flow levels were taken from the output of the extracted input dataset, which was obtained by choosing representative 20 surface observation sites' data and two upper level temperature and two radiosonde data out of 186 surface and ten upper air observations. The flow levels those are compared were illustrated in the following figures,

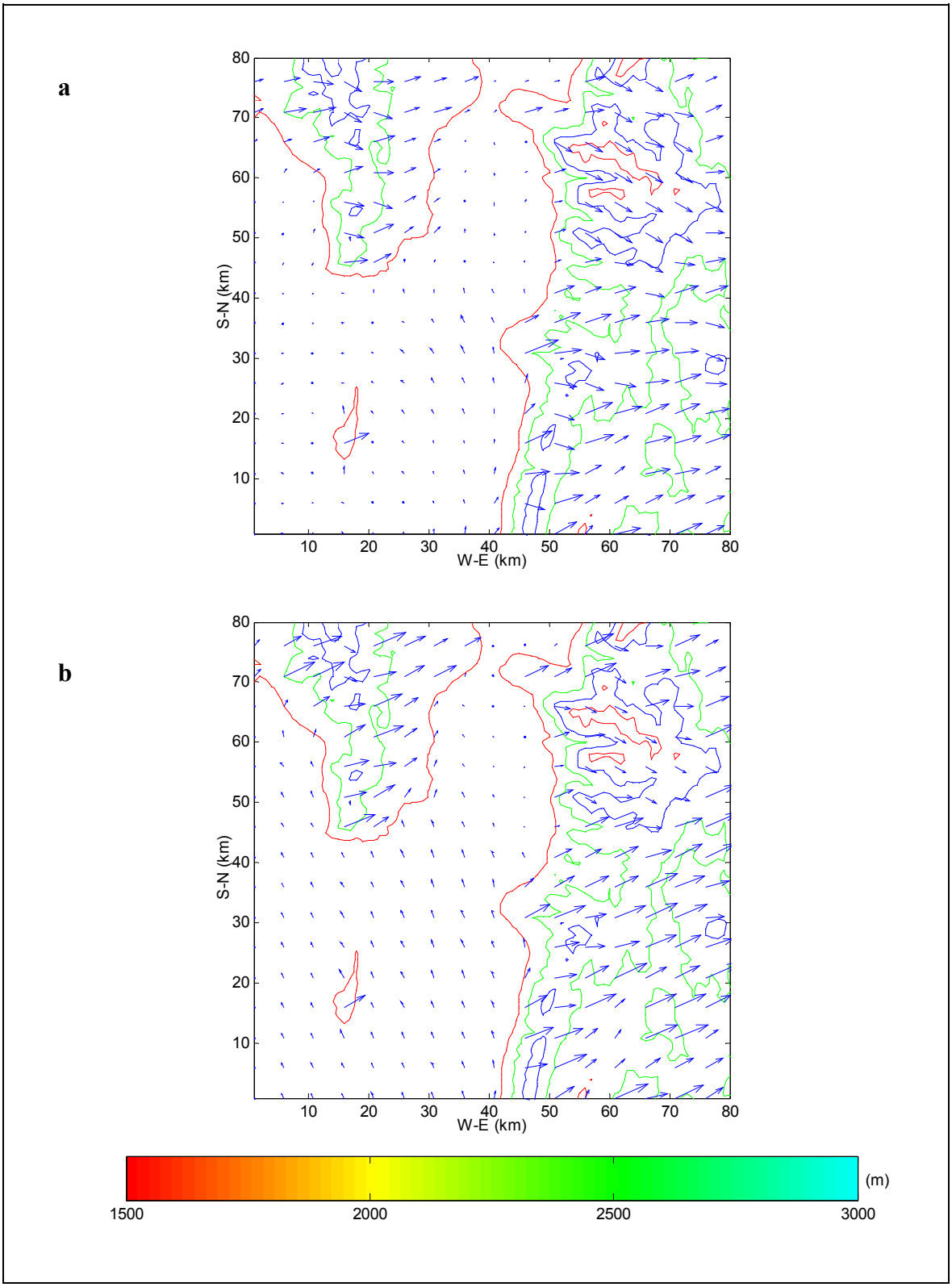

Figure 5.3 WOCSS wind scheme analysis at the height of 1400 m above sea level, (a) with the sample dataset, (b) with the extracted dataset

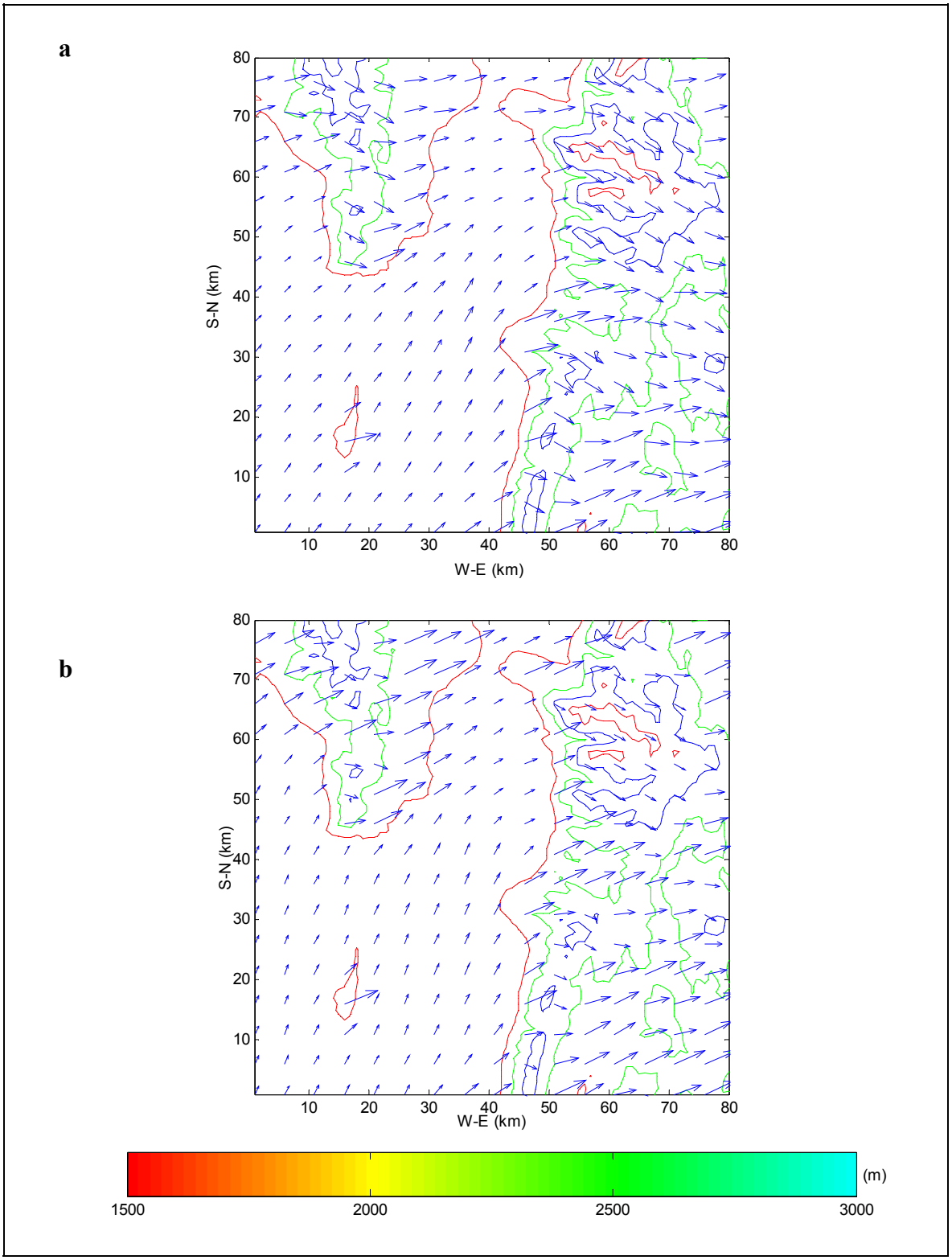

Figure 5.4. WOCSS wind scheme analysis at the height of 1600 m above sea level, (a) with the sample dataset, (b) with the extracted dataset

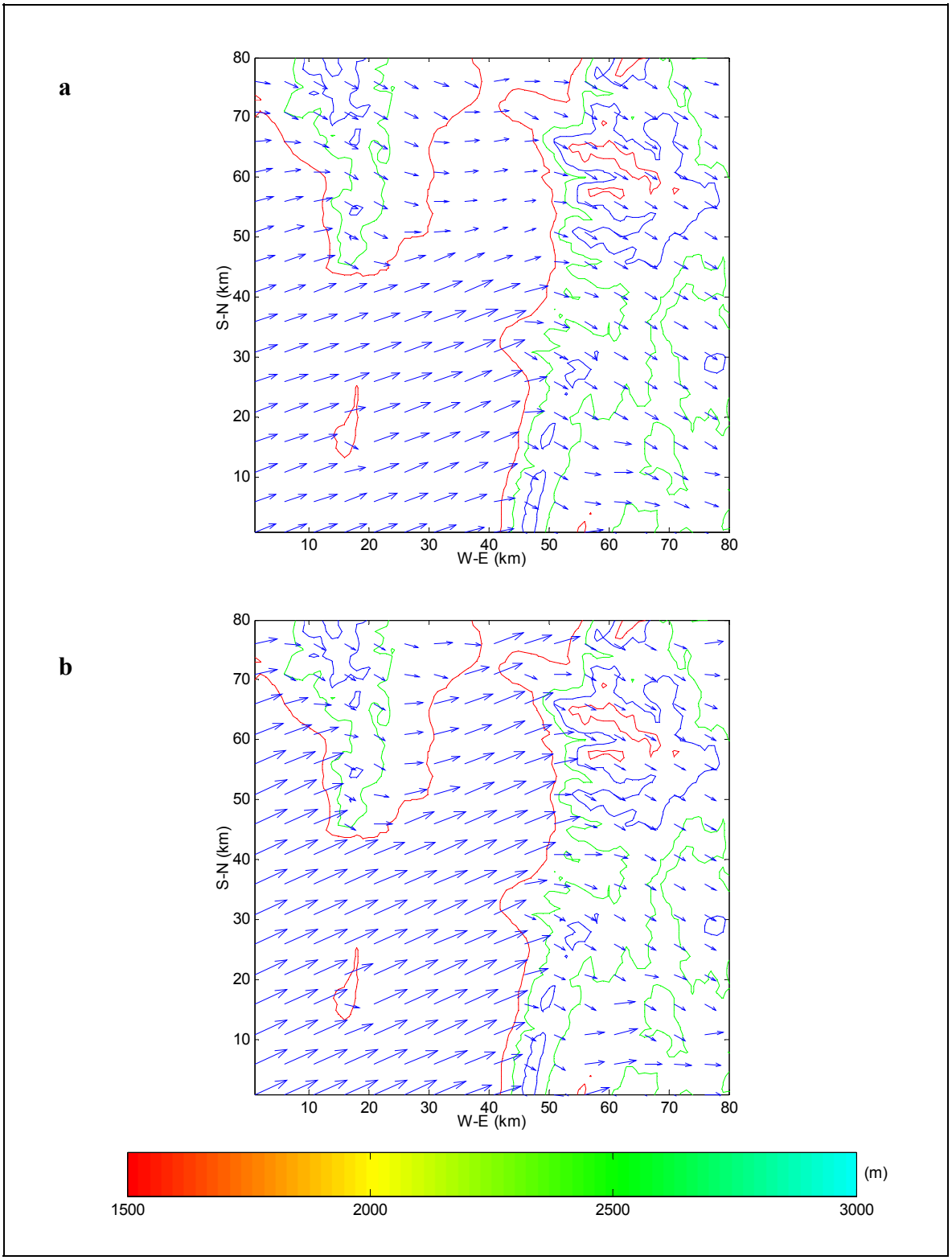

Figure 5.5. WOCSS wind scheme analysis at the height of 2000 m above sea level (a) with the sample dataset, (b) with the extracted dataset

As it can be seen from the Figures 5.2 – 5.4, the decrease in the number of data that is given as an input, results slight differences. The flow pattern is generally conserved whereas the wind speed decreases in small amount with the decrease in number of data in the input. These conclusions are consistent with Ludwig and Sinton's study (Ludwig and Sinton, 2000).

The streamline plots of the wind fields will show the flow patterns and whether they are conserved or not.

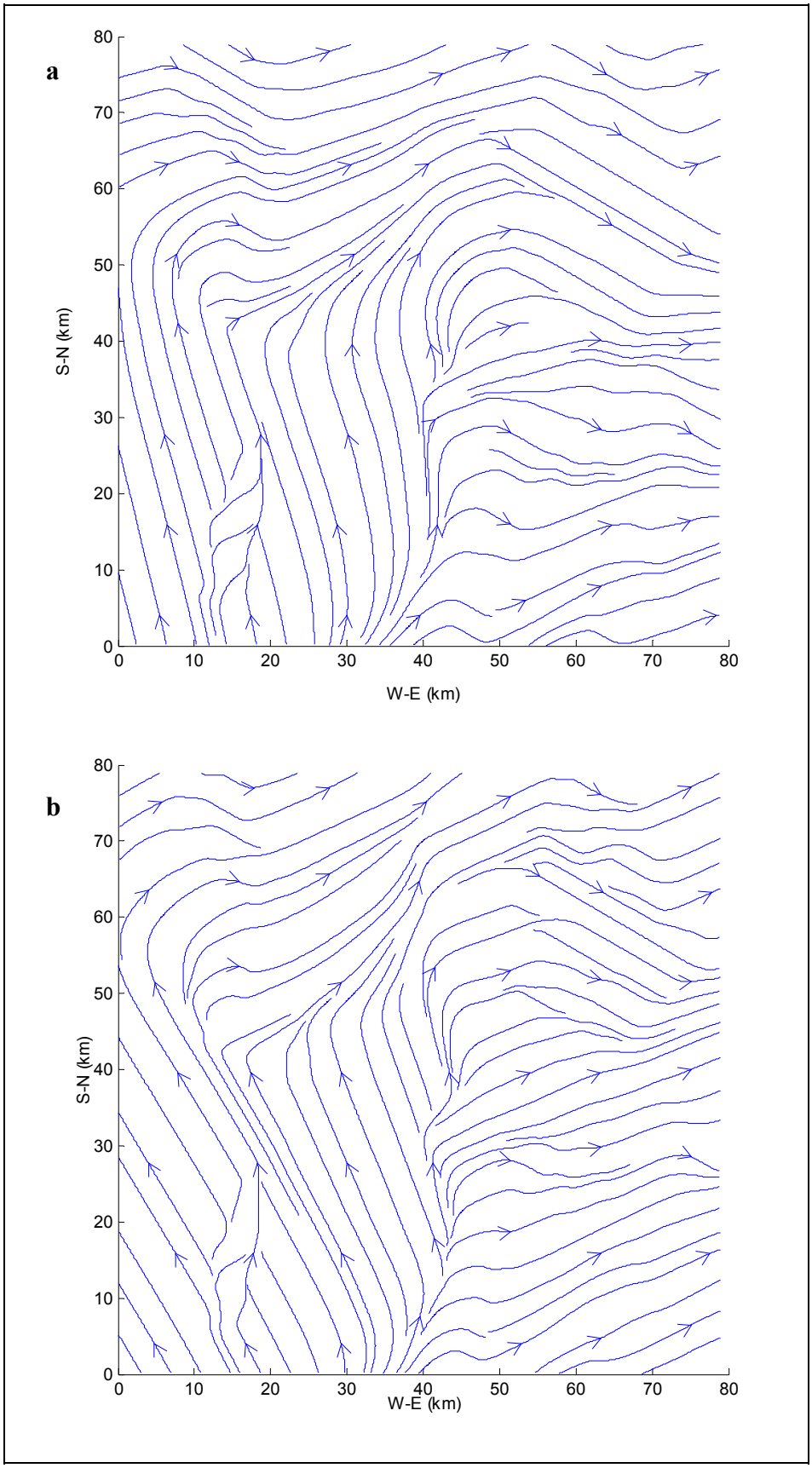

Figure 5.6. Streamline plot of results of sample (a) and extracted (b) datasets at 1400 m

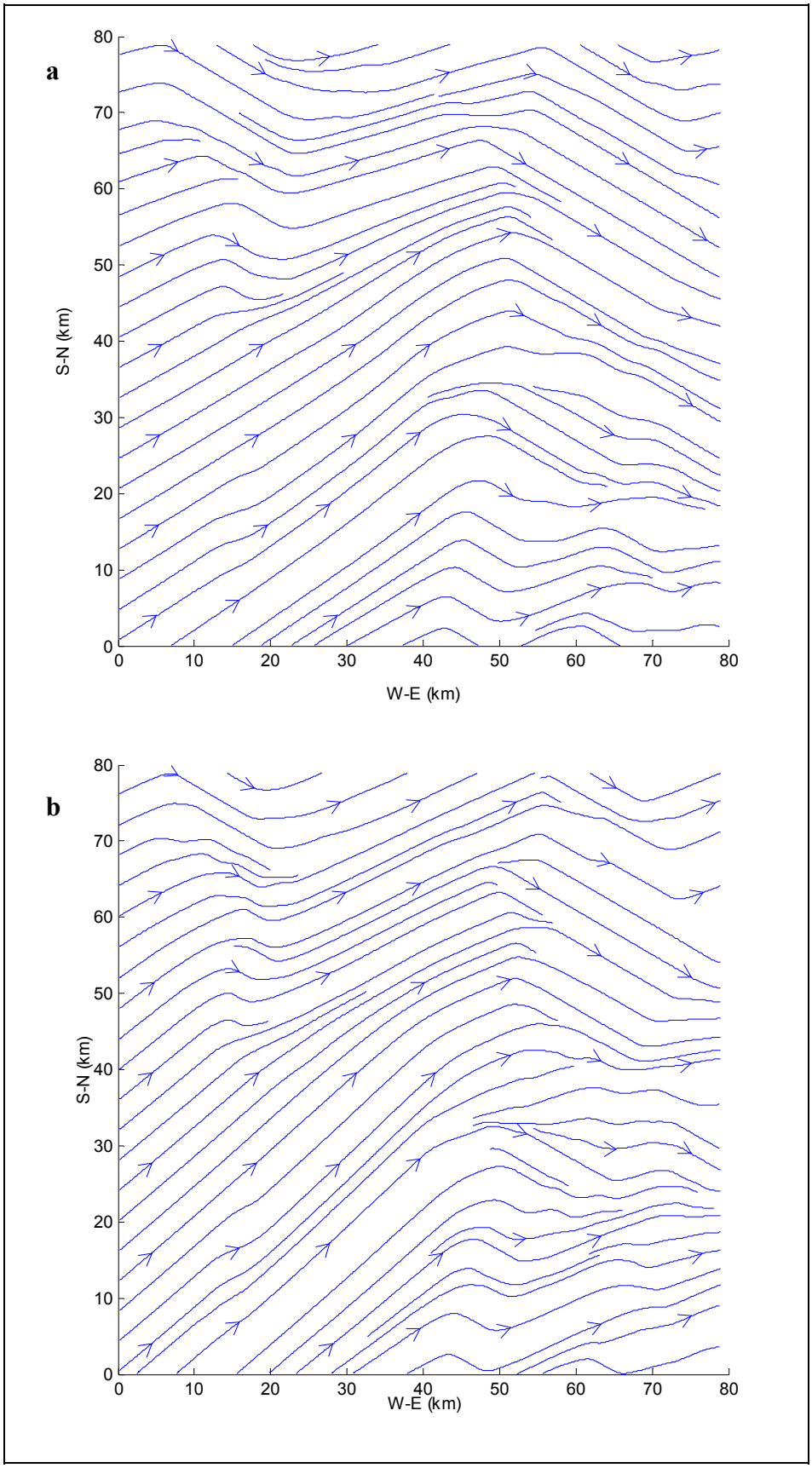

Figure 5.7. Streamline plot of results of sample (a) and extracted (b) datasets at 1600 m

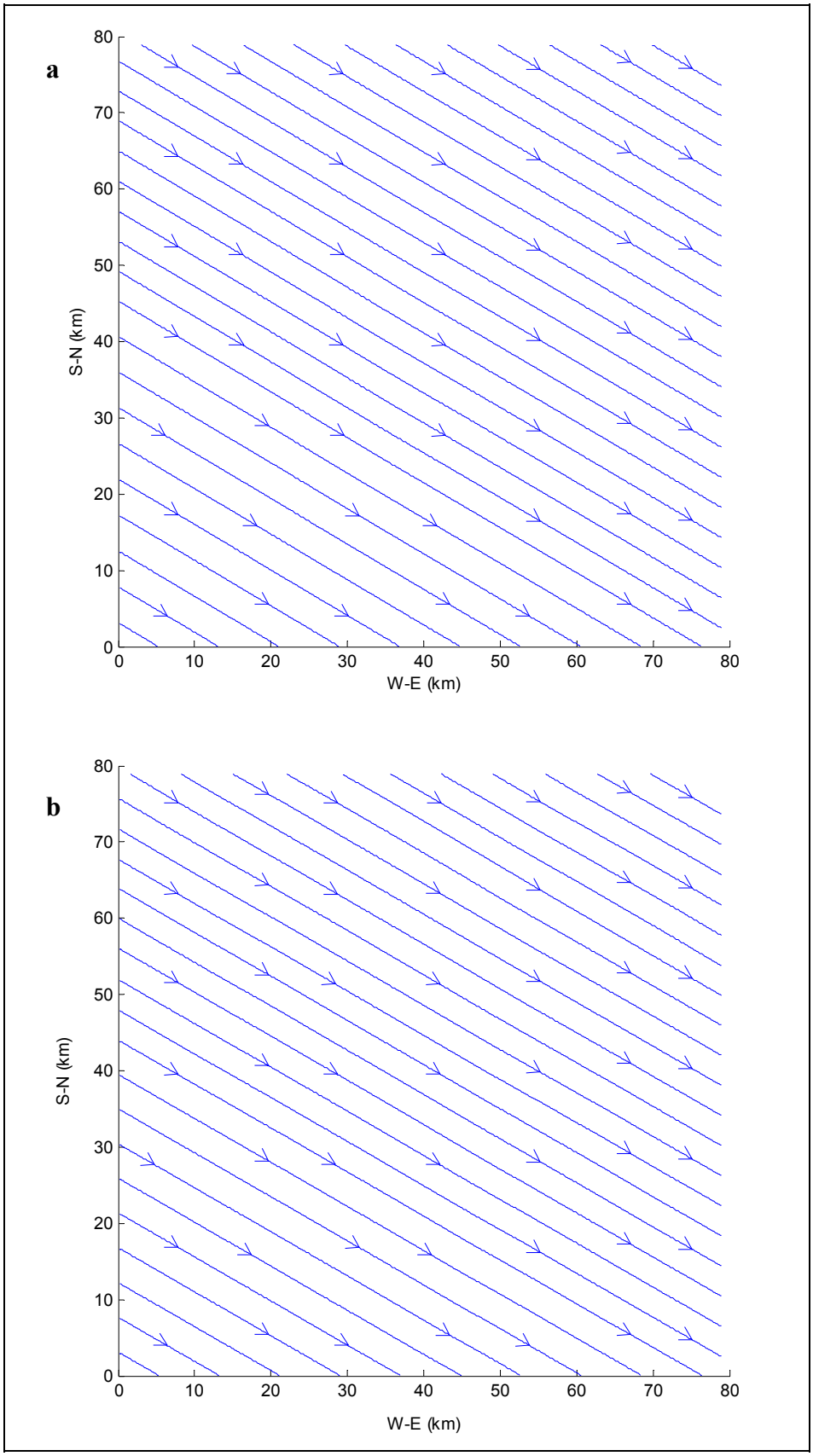

Figure 5.8. Streamline plot of results of sample (a) and extracted (b) datasets at 2000 m

Figures 5.6 – 5.8 show that, the pattern of the flow preserves its main features although number of observation sites is reduced in the input. As well in Figure 5.8 with the increase in height of the flow surface levels, the effect of terrain disappears, as expected.

5.2. APPLICATION OF WOCSS TO BOSPHORUS

The applicability of WOCSS to Bosphorus with relatively less observation sites was tested and it was concluded that the scheme is applicable. Four surface observations and one upper level air observation were supplied by Boğaziçi University The Kandilli Observatory and Earthquake Research Institute and National Oceanic and Atmospheric Administration (NOAA) within U.S. Department of Commerce, respectively. NOAA is a federal agency focused on the condition of the oceans and the atmosphere.

Surface observations include temperature, pressure and wind direction and speed data for the altitude ten meters above of the observation sites' location. Five different surface temperature data were taken daily from each observation site. The two temperature data were the minimum and the maximum values during the day and the other three were taken at 05:00, 13:00, and 21:00, respectively. The pressure data were available at 12:00 for each day. The wind was observed at the beginning of every hour in a day; speed, direction and horizontal components of the wind velocity were reported. All these data were taken simultaneously from Florya, Göztepe, Kireçburnu and Kumköy observation stations.

Routine meteorological Göztepe radiosonde were archived at twelve hour intervals in a day. These data are available at the website of NOAA (Radiosonde Database Access). The radiosonde data were taken at Göztepe and comprised the information about pressure, temperature, dew point and direction and speed of wind for different heights. The radiosonde data are available at 00:00 and 12:00 for each day. The identifiers of upper air and surface observation sites are given in Table 5.1.

Table 5.1. Observation sites

Station locations	Station ID	Longitude	Latitude	UTM zone 35		Elevation (m)
				East (km)	North(km)	
Florya	17636	28.80	40.98	651.43	4538.10	34.00
Göztepe	17062	29.08	40.97	651.45	4536.99	33.00
Kireçburnu	17061	29.05	41.14	672.05	4556.99	39.00
Kumköy	17059	29.02	41.15	669.50	4557.38	5.00

One of the other necessary data to run the WOCSS code was the digitalized elevation data of the domain. The digitalized terrain data were available at the web site of United States of Geographical Survey (USGS). The data were available in different resolutions. WOCSS code uses one-kilometer grid size in calculations so the elevation data were required for every one kilometer. For the area of interest, one kilometer was considered to be equal to 30 arc-seconds difference between two longitudes as well two latitudes. Global 30 Arc-Second Elevation Data Set (GTOPO30) is a global raster Digital Elevation Model (DEM) with a horizontal grid spacing of 30 arc-seconds (approximately 1 kilometer), which is provided at the website of USGS. GTOPO30 was derived from a variety of raster and vector sources (United States of Geographical Survey). Since GTOPO30 is global digital elevation model, to take out terrain information of the area of interest, it was necessary to write a short subroutine with using built-in functions of mapping toolbox in MATLAB programming language.

The area of interest begins with the latitude and longitude of 40.95° N and 28.82° E and covers an area that lies 40 km in both east and north direction. Since WOCSS code uses coordinates of The Universal Transverse Mercator (UTM) grids, the reference point of the domain was converted to UTM coordinates and the following values were obtained 653,180 E and 4,534,800 N in the UTM zone 35 T.

The application of WOCSS to Bosphorus was performed for datasets belonging to dates 18 August, 11 October and 10 December 1998. All the observed air qualities should be reported simultaneously in order to be used as an input to the WOCSS. Since the only

available simultaneous air observation data from all five stations were the ones which were reported at 12:00, this dataset was chosen for the application of WOCSS to Bosphorus.

The results of WOCSS analysis scheme for Bosphorus on dates 18 August, 11 October and 10 December are given in the following figures, respectively.

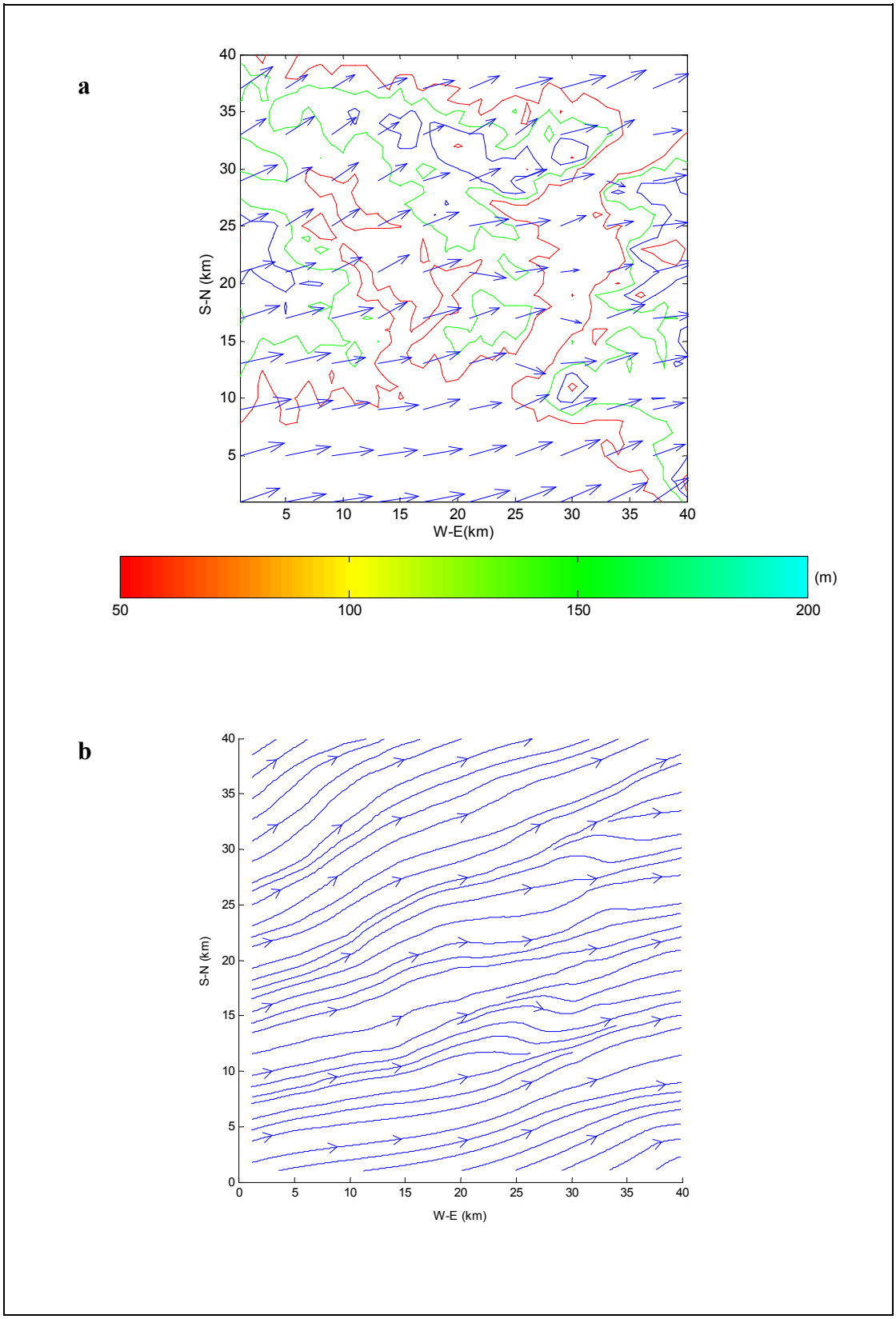

Figure 5.9. The vector (a) and streamline (b) plots of the second flow surface for 10 December

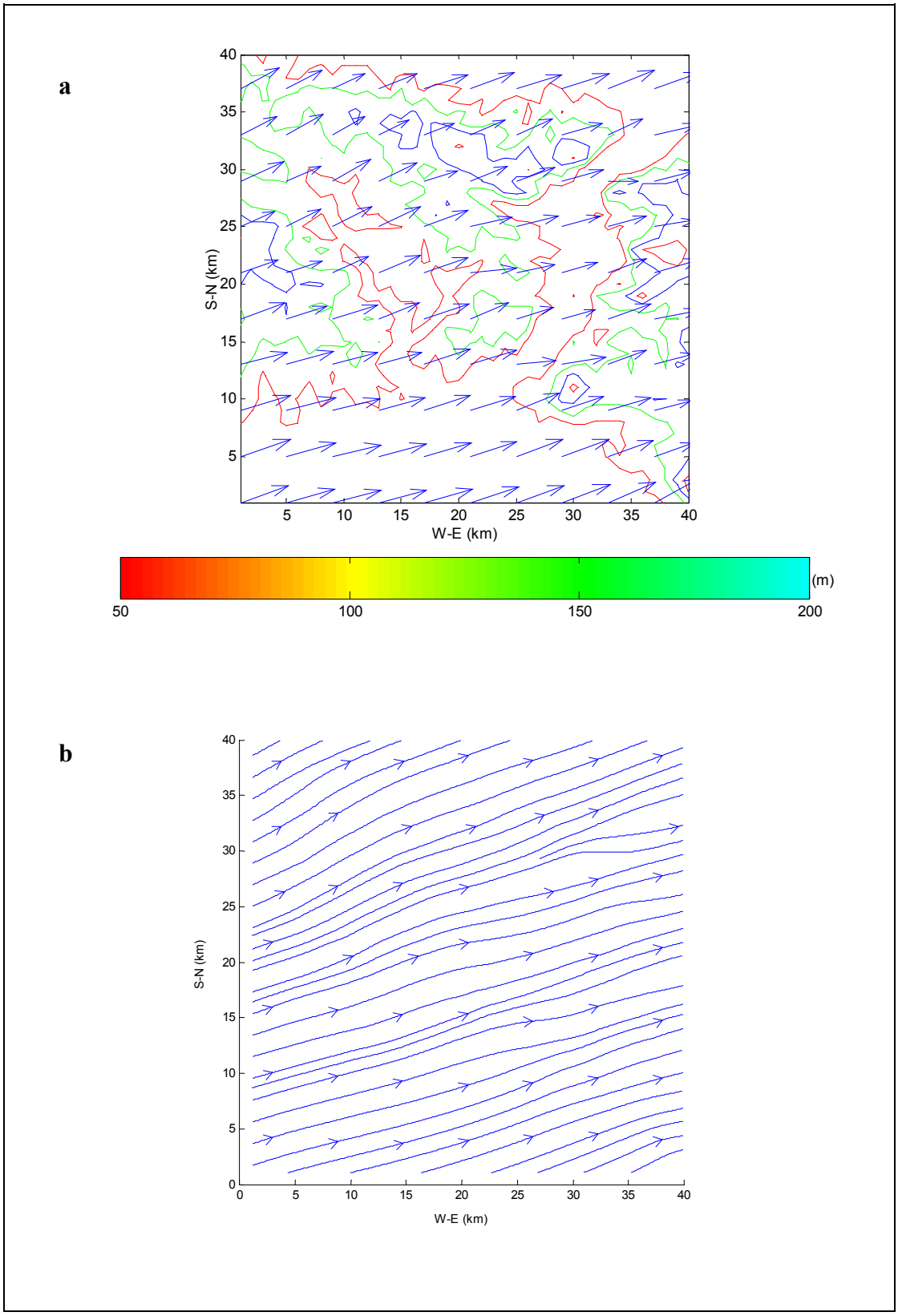

Figure 5.10. The vector (a) and streamline (b) plots of the forth flow surface for 10 December

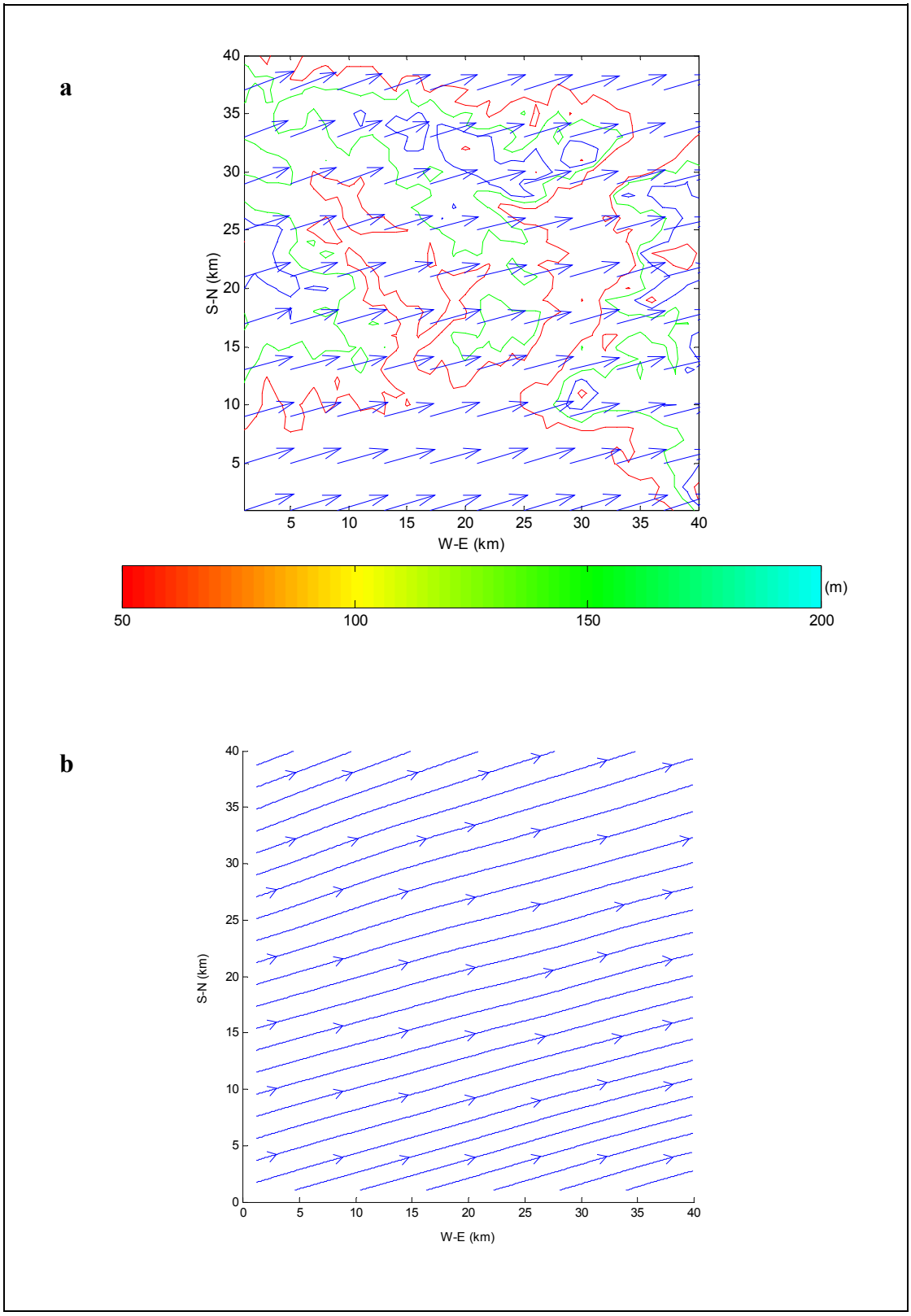

Figure 5.11. The vector (a) and streamline (b) plots of the eighth flow surface for 10 December

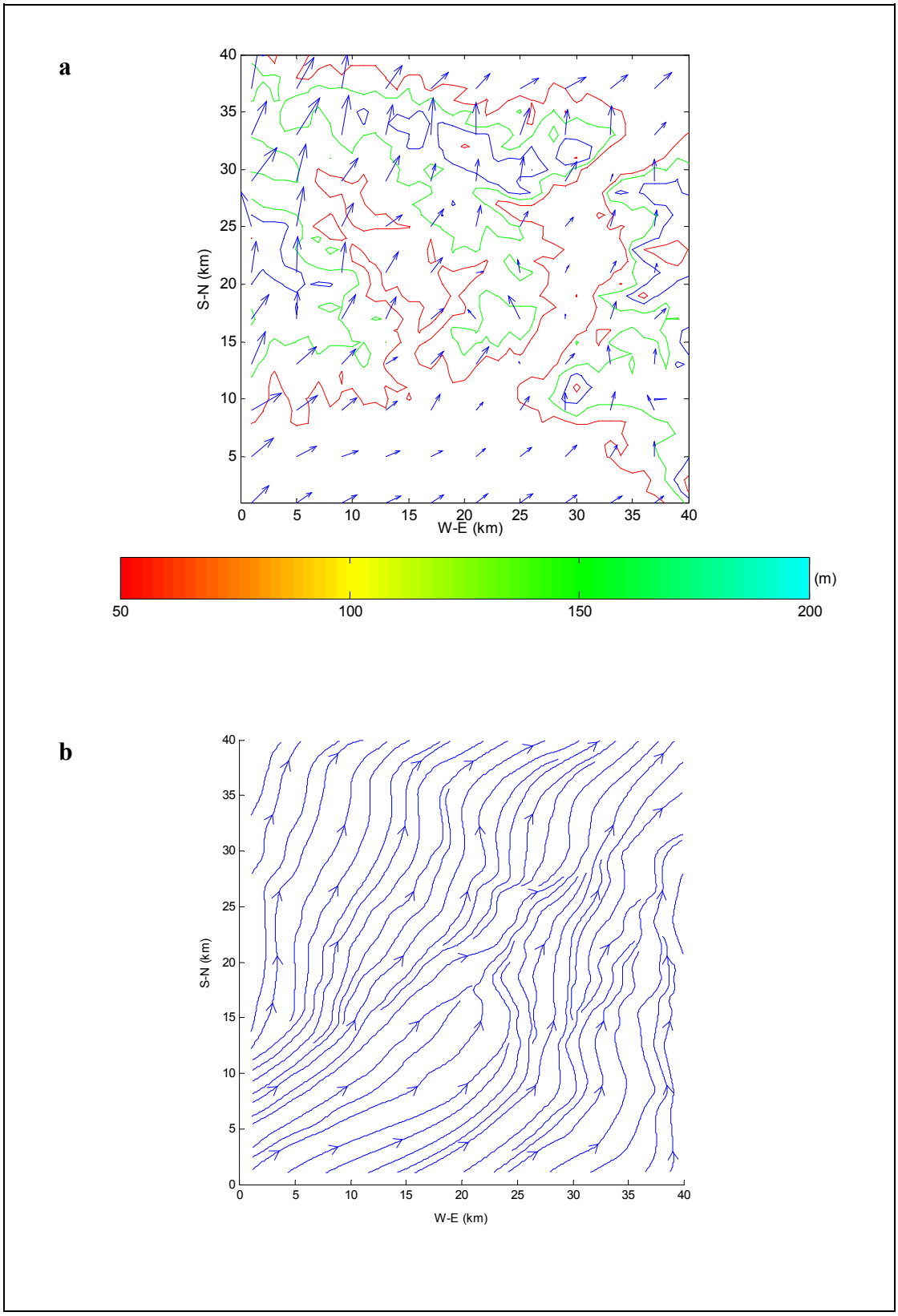

Figure 5.12. The vector (a) and streamline (b) plots of the second flow surface for 11 October

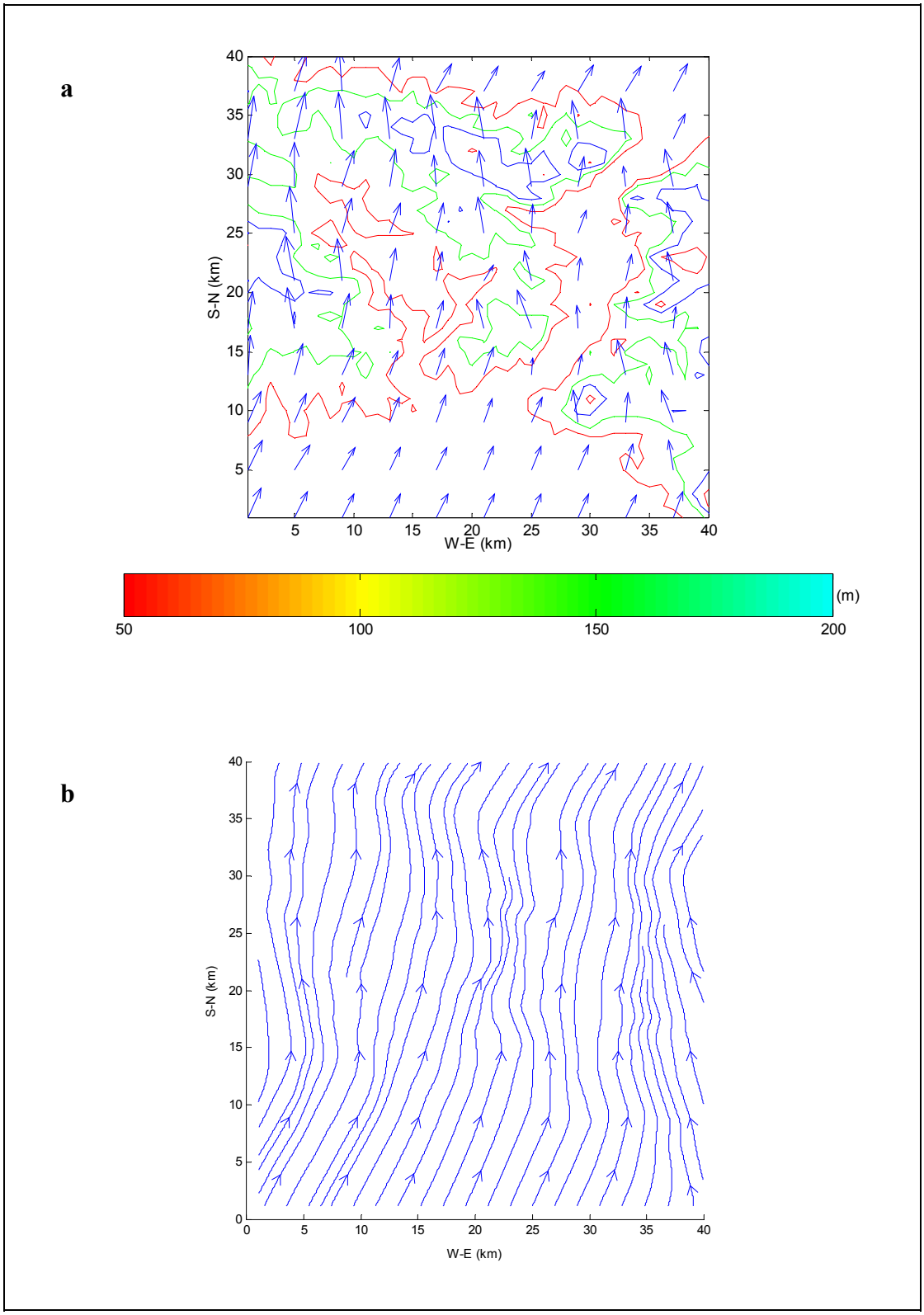

Figure 5.13. The vector (a) and streamline (b)plots of the fourth flow surface for 11 October

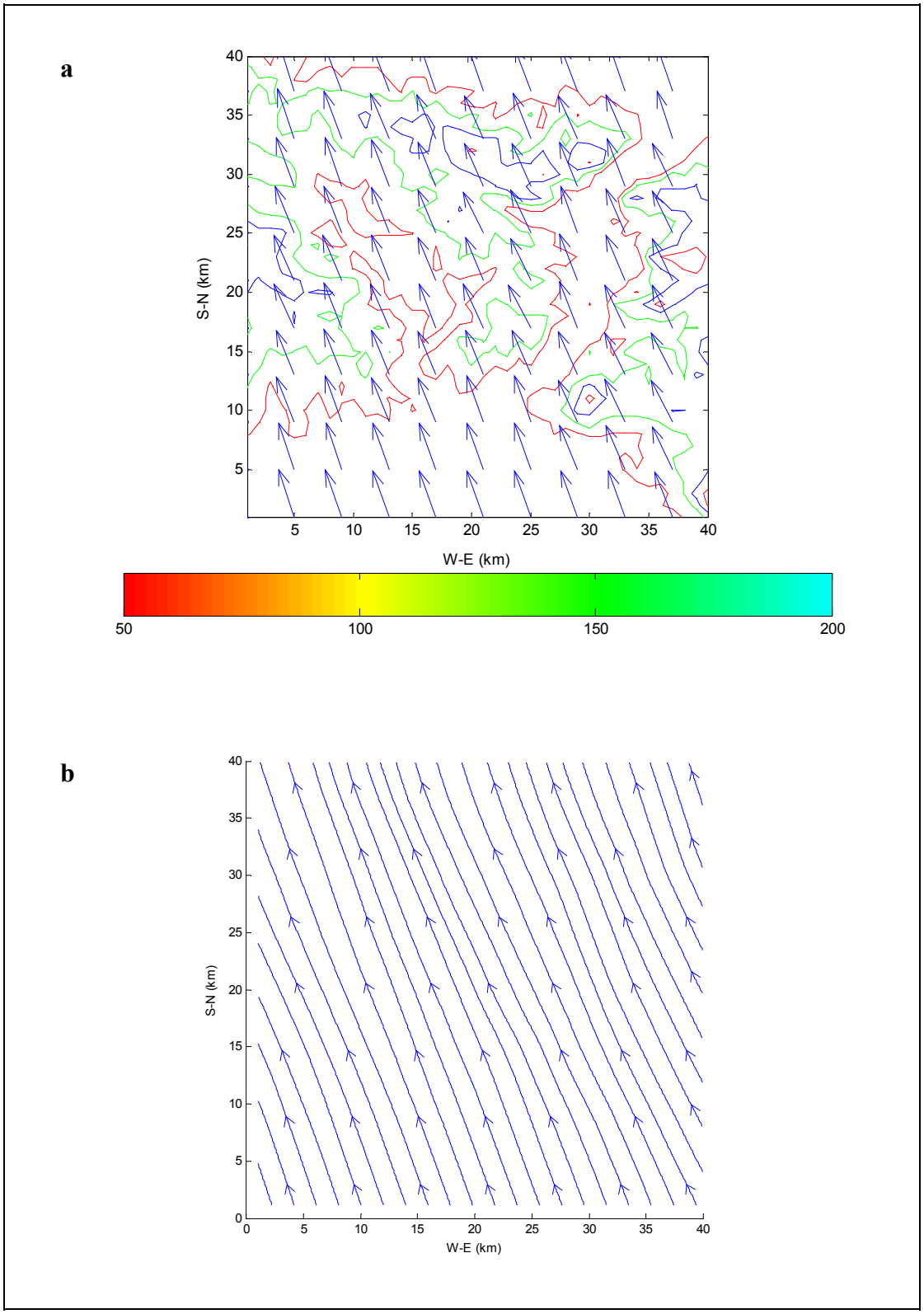

Figure 5.14. The vector (a) and streamline (b) plots of the eighth flow surface for 11 October

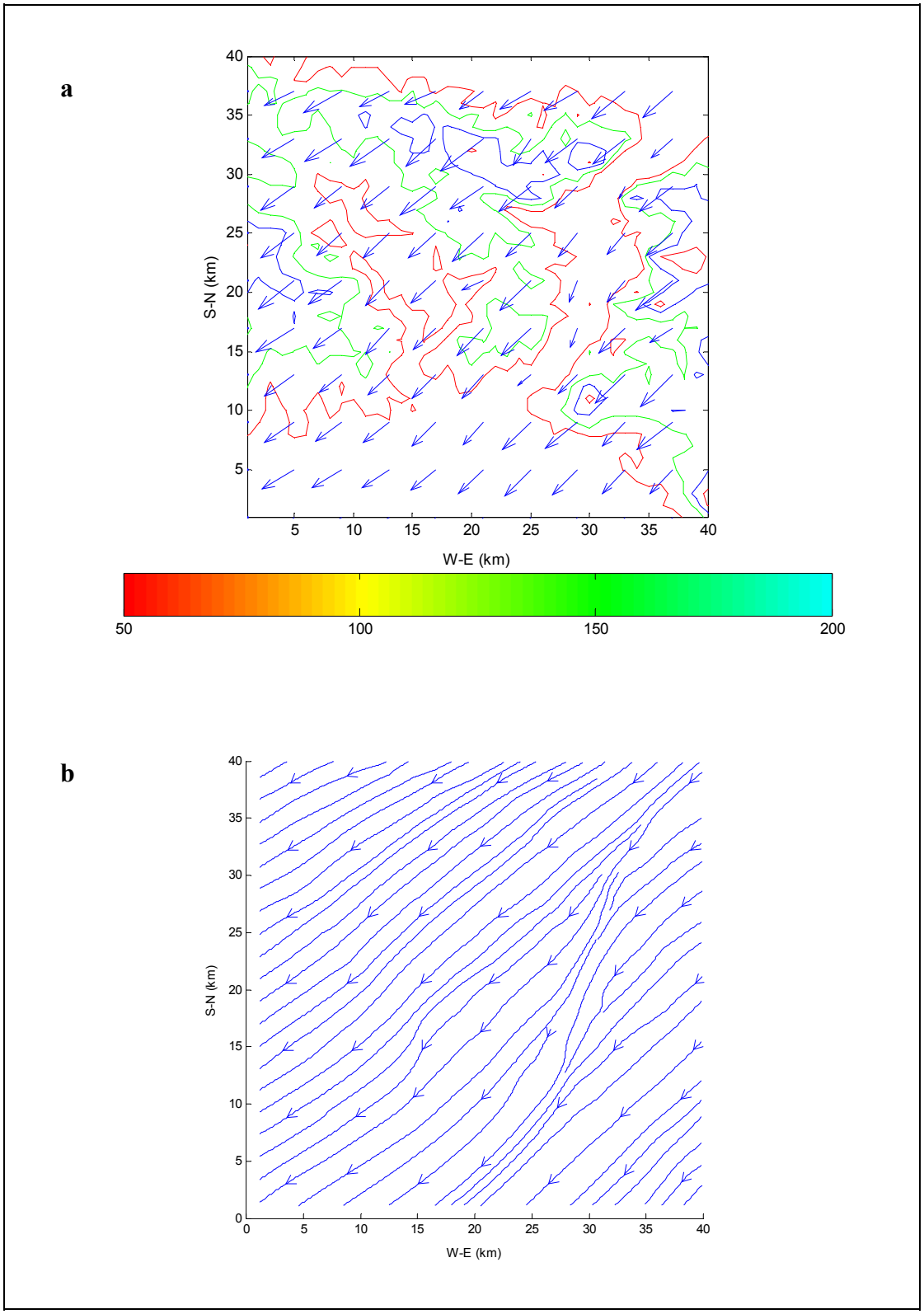

Figure 5.15. The vector (a) and streamline (b) plots of the second flow surface for 18 August

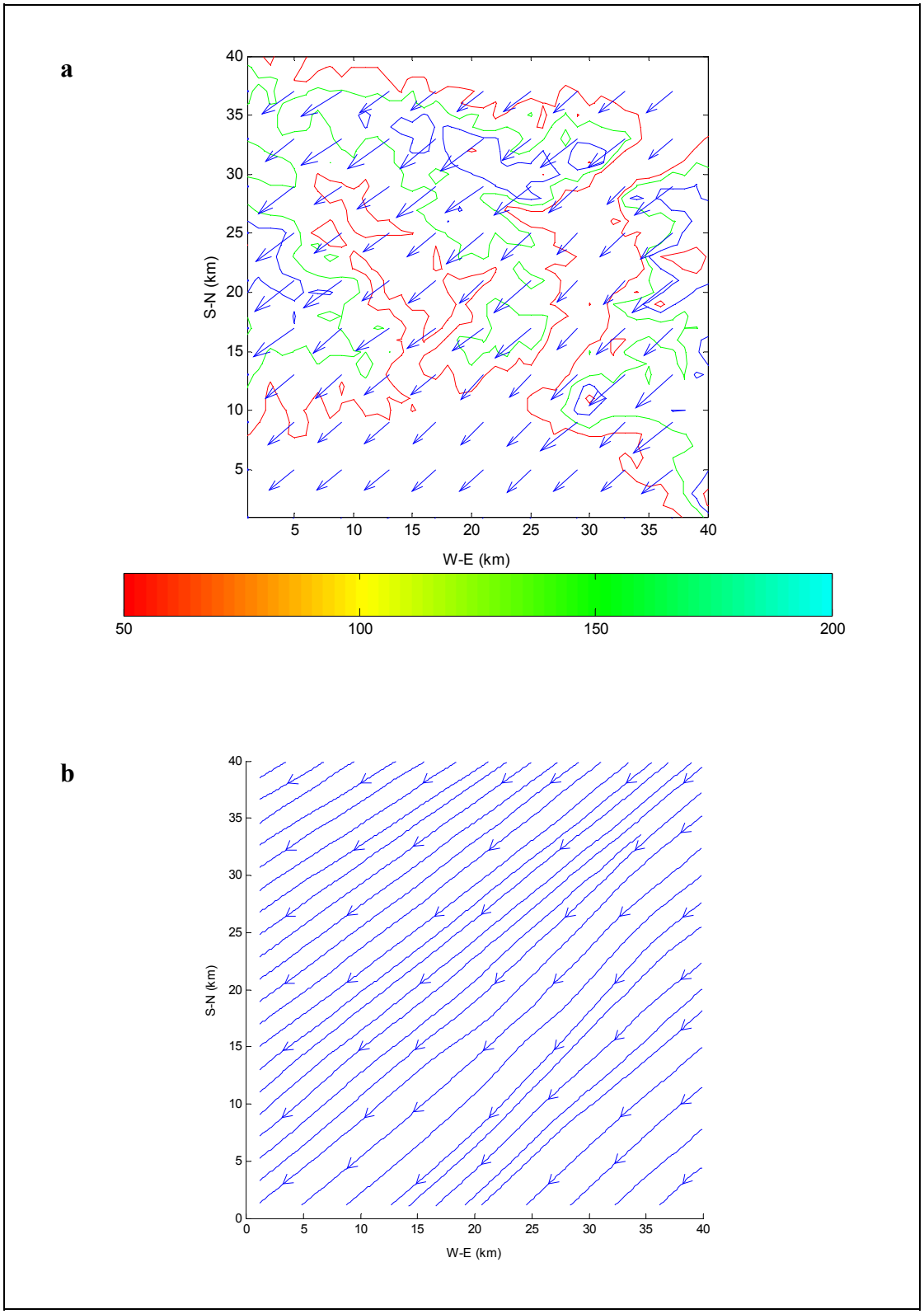

Figure 5.16. The vector (a) and streamline (b) plots of the fourth flow surface for 18 August

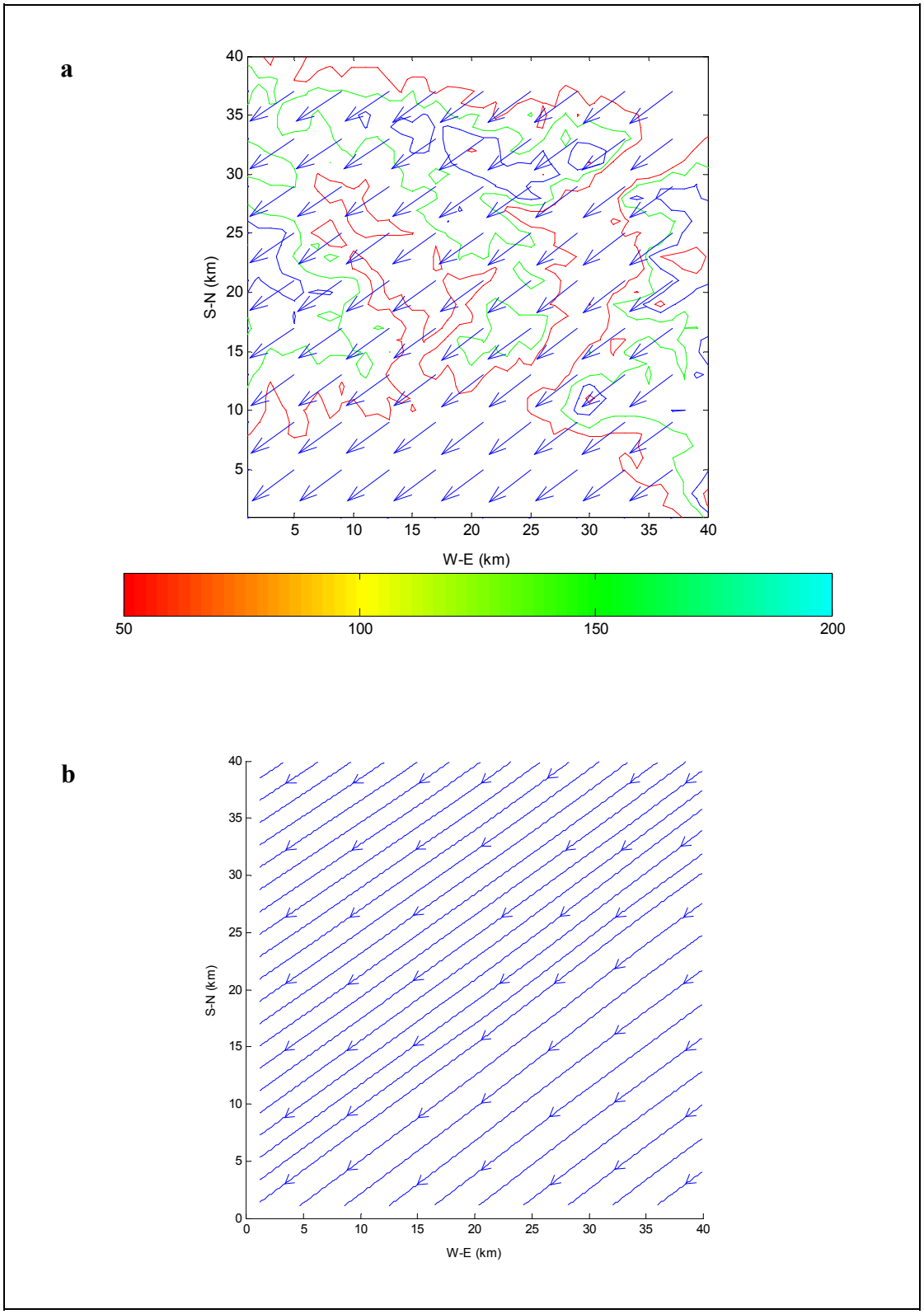

Figure 5.17. The vector (a) and streamline (b) plots of the eighth flow surface for 18 August

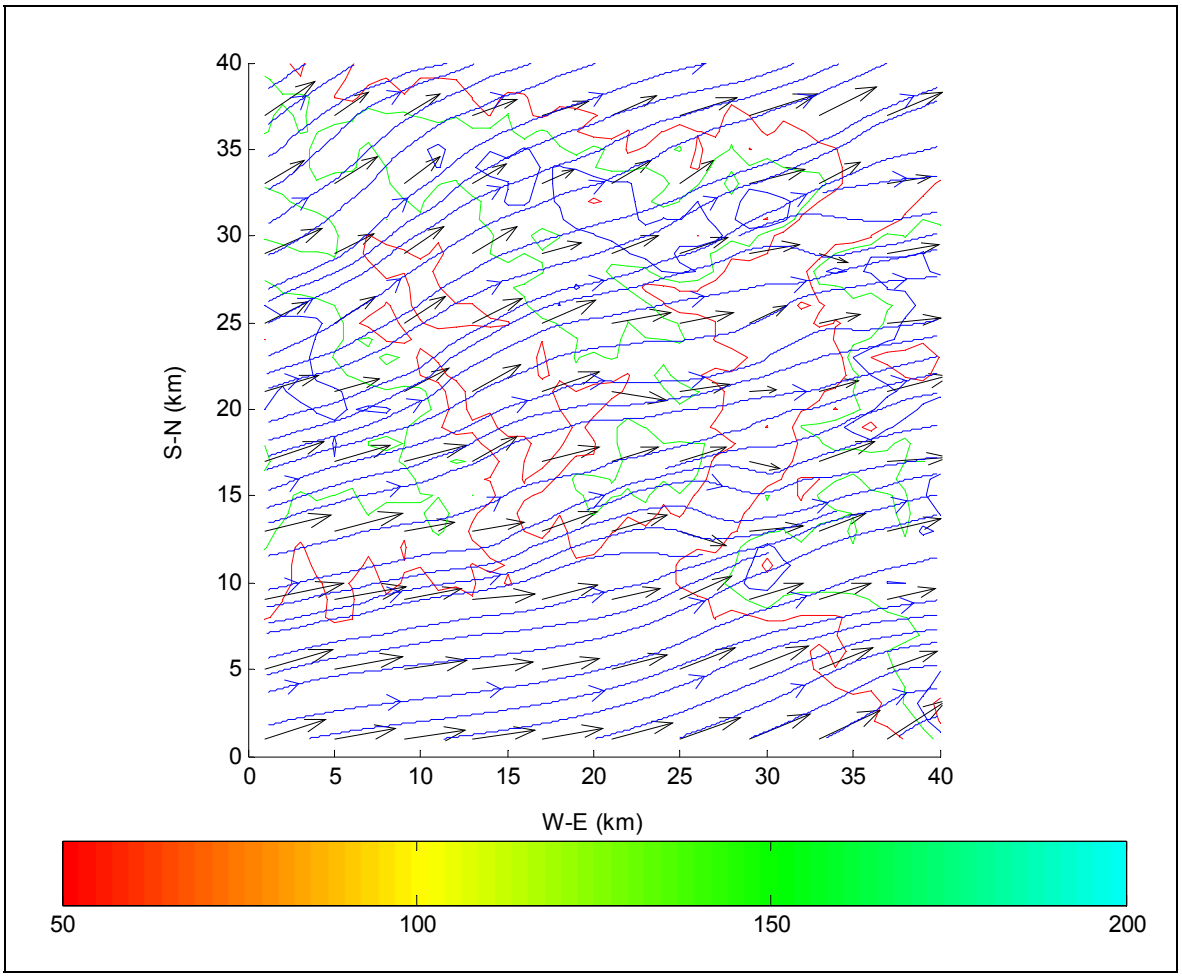

Figure 5.18. The superimposed vector and streamline plots of second flow level for 10 December

There are several factors that might affect the degree to which the WOCSS results reflect the actual wind field. For WOCSS, the number of inputs used will be very important. Another characteristics of the model that might affect performance is the number and height of the surfaces defined. If there are too few levels or they are too high, then they will pass over the terrain and terrain effect on the wind would not have been simulated.

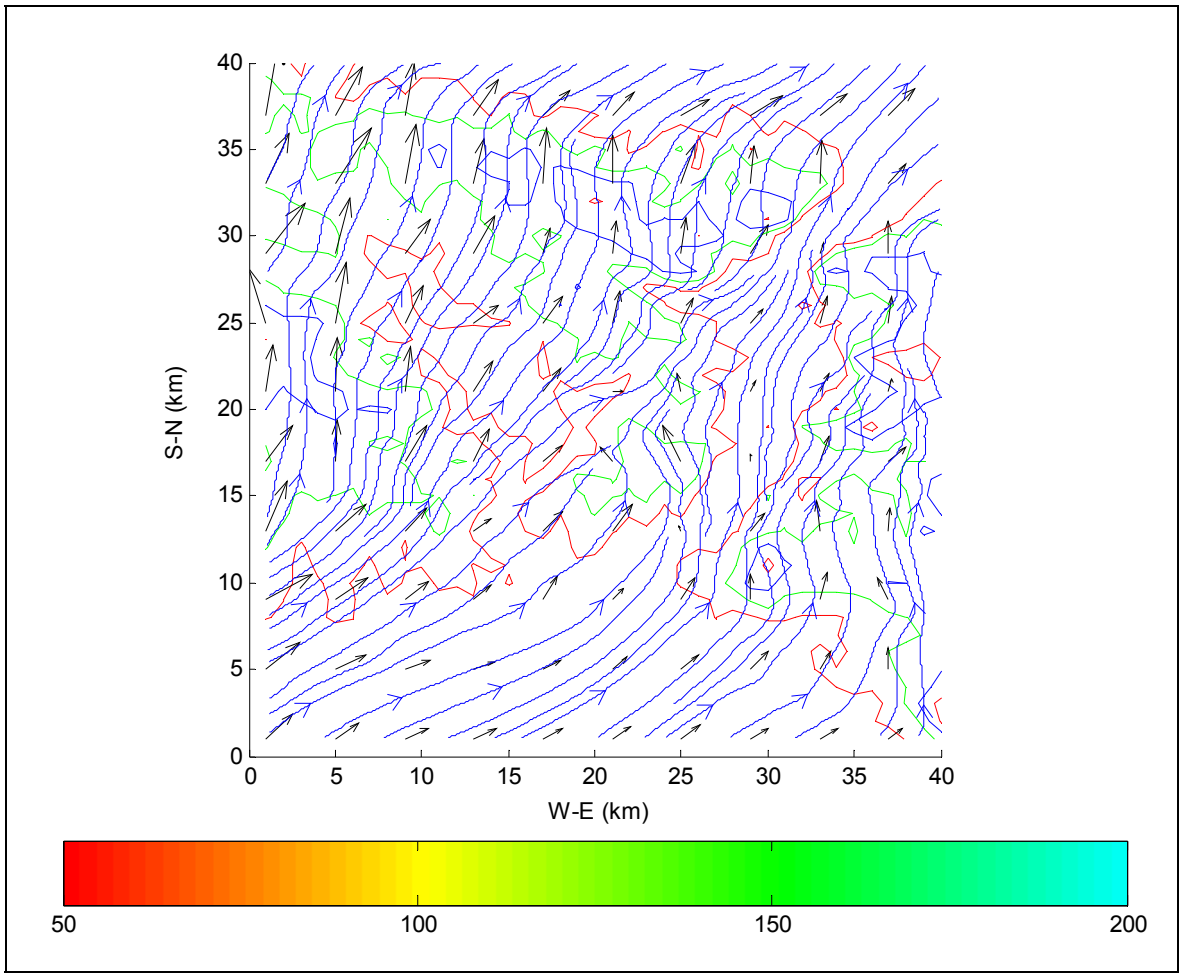

Figure 5.19. The superimposed vector and streamline plots of second flow surface for 11 October

As it was mentioned before, the number of the surface sites and their location were able to represent the domain and one upper air observation satisfied the minimum requirement of the model. In fact, the minimum number of surface sites is defined to be four in Ludwig and Sinton's study (Ludwig and Sinton, 2000). However, in that study, all the model calculations were made on a 108 × 103 grid with spacing of one kilometer where as the specified domain in this study was performed on a 40 × 40 gird with the same size of grid spacing. So the number of surface sites could be considered acceptable.

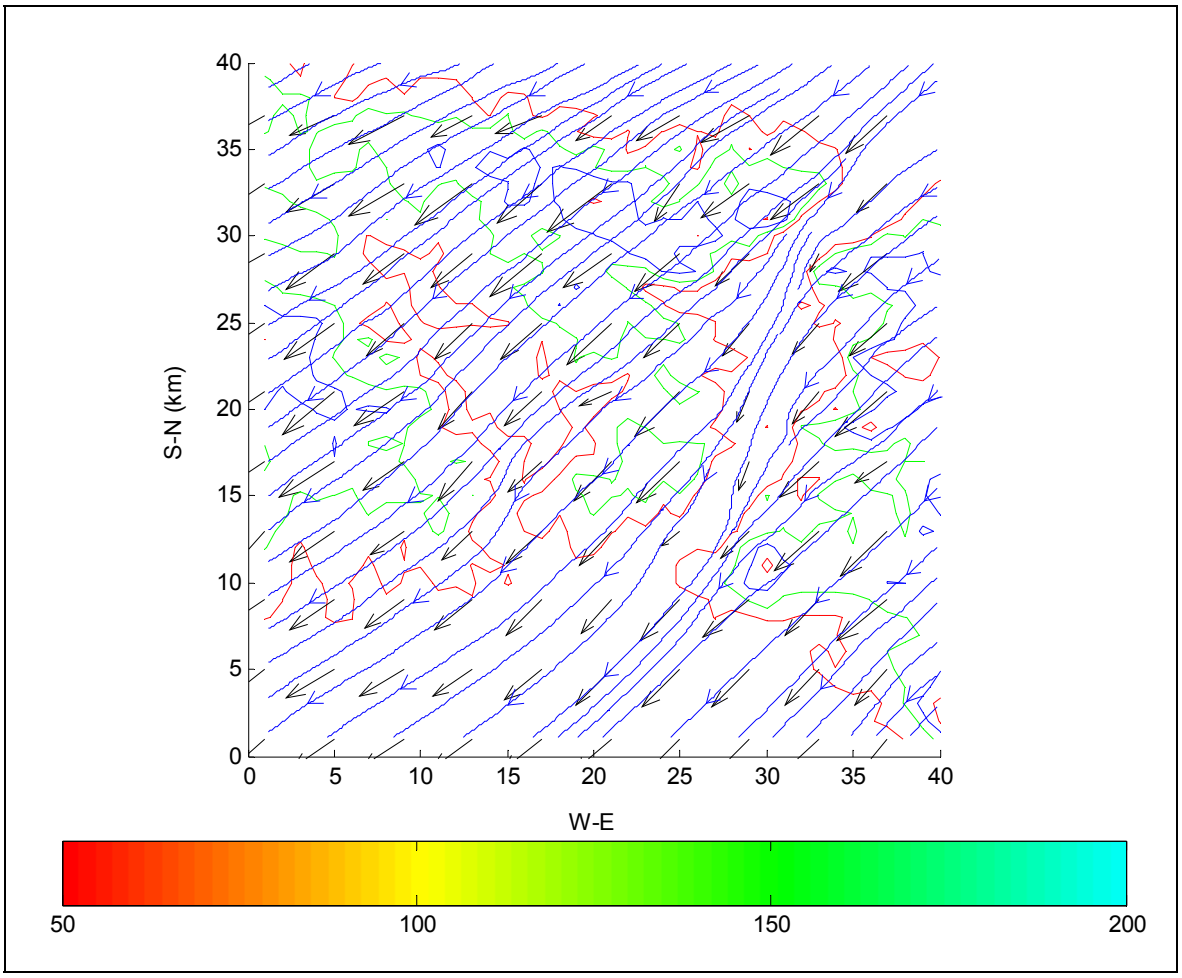

Figure 5.20. The superimposed vector and streamline plots of second flow surface for 18 August

It was chosen to run WOCSS using eight levels. These levels are defined over the lowest terrain, the sea levels areas in this case. The heights used for calculations with eight surfaces were 10 (surface winds), 50, 100, 150, 200, 300, 400, 600, 1000 meters. The range of height covers the extent of the terrain in Bosphorus area with the highest terrain at the 244 meters. As it may be seen from figures, especially streamline plots, of fourth flow levels for all three dates, the effect of the terrain begins to disappear even at the elevation of 150 meters and the figures belonging to eighth flow levels clearly shows that at the height of 600 meters, terrain effect almost completely disappears.

In Figure 5.12, a week south-west (SW) flow for the second flow level case can be seen while in Figure 5.15, a strong north-east (NE) flow at the same flow level was shown.

For the strong NE flow in 18 August a little tendency was noted for flow deflection around higher elevation and through Bosphorus strait. In part this is due to prevailing wind direction being closely aligned with the northeast-southwest oriented terrain features. The weak flow case at 10 December case was more noticeably characterized by flow guided by terrain features. Flow is funneled through Bosphorus strait. This phenomenon was also observed at 18 August however when the streamline plots of this two case was analyzed for the second flow level in Figures 5.14 and 5.11 for the case weak SW flow and strong NE flow, respectively. It was clearly seen that the channeling through Bosphorus strait is stronger in the weak SW flow case then in the NE flow case. Inspection of vector plot of weak SW flow case in Figure 5.17 showed that large wind direction changes between Kireçburnu and Kumköy observation sites although the distance between them is short. Given this fact, the WOCSS can be judged to have performed well in analyzing winds here.

Another interesting result of the weak SW flow case at 18 August is while the wind direction near the surface was south-west, wind begins to change its direction to south east. This fact is clearly illustrated as the vector plots of three different flow surfaces in Figures 5.12 – 5.14. Also, it is remarkable that the terrain effect on the flow is more noticeable in this case then in the other two. Even in the fourth flow level, the terrain effect is still visible whereas in the other two cases terrain effect for the same level is inconspicuous.

For the strong west flow in 10 December at the height of 100 meters, the split points appear in the flow near the higher elevations. This split points can be seen at the vector plot in Figure 5.9. The model often misses the location of split in the flow then the difference between observed and calculated direction may be as much as 180º. So on the one hand it is good WOCSS to simulate the splits in the flow but in the other hand the splits might be simulated deficiently.

6. CONCLUSIONS AND RECOMMENDATIONS

The WOCSS meteorological model was used to produce three-dimensional gridded fields of winds on Bosphorus. The results simulated by WOCSS were visualized in MATLAB environment.

The meteorological data required by WOCSS were taken from four surface observation sites and one upper air observation site. Surface air observation data were taken from Florya, Göztepe, Kireçburnu and Kumköy stations. The radiosonde data were reported at Göztepe station. All the stations are located inside the model domain and they are spread out through the domain so to represent terrain features.

The digitalized terrain elevation data were obtained from the official website of United States of Geographical Survey (USGS). For the purpose of study, Global 30 Arc-Second Elevation Data Set (GTOPO30) which has a horizontal grid spacing of 30 arc-seconds (approximately one kilometer) was chosen. Since GTOPO30 is global digital elevation model, to take out terrain information of the area of interest, it was necessary to write a short subroutine with using built-in functions of mapping toolbox in MATLAB programming language.

The WOCSS model was performed using a sample data set, which was supplied by Prof. Ludwig, and an extracted data set from this sample by reducing the number of available data in the given data set. The obtained results show a negligible deviation and thus, were satisfactory. Then, the WOCSS model was performed on Bosphorus for three different data set belonging to 18 August, 11 October and 10 December.

The strong NE flow and weak SW flow were compared. The evaporation in August acts as a source of convective heat transportation. This phenomena yields the atmosphere to be near or neutral stable. Under this condition, the flow is not constrained to go around higher obstacles. So, the effect of terrain on the strong NE flow is relatively less. Whereas in the case of weak SW flow on the date 11 October, the terrain effect is more obvious.

Since the occurrence of the temperature inversion which can be easily seen in radiosonde data for this date, constrains the flow to be on terrain following coordinates. So, the weak SW flow case is more apparently characterized by flow guided by terrain features.

In case of strong west (W) flow, near the higher elevations, the flow splits were observed. But as it was mentioned in the study of Ludwig and Sinton (2000), near these split points WOCSS needs observation sites in order to be able to simulate actual wind fields.

All three cases showed that for Bosphorus area the terrain effect almost disappear at the height of 600 m. The results were said to be satisfactory in this aspect. However, it had been desired to have data from more different located stations. So, it would have been possible to compare the observed and simulated winds.

Another interesting result is eighth flow level of 18 August case, while the weak surface winds are blowing in the south-west direction at the height 600 m, the flow was strong and directed in the south-east direction. However, there is only one available sounding data, it is not possible to check this flow surface.

The WOCSS model has proven quite easy to use and does not require large computing resources for operation. All the results reported here were obtained in the limits of real time.

The major conclusion to be drawn is that reasonable wind analysis can be performed by using WOCSS. As it is always true with diagnostic models, the results may be improved by the more input wind data. However, with provided data for this study, the terrain effect on the flow was able to be simulated, and it was concluded that the dispersion or turbulence estimation models which require a three-dimensional gridded wind field can use the results of WOCSS as input.

REFERENCES

Astrup, P., T. ,Mikkelsen, and N. O. Jensen, 1997, "A Fast Model for Mean and TurbulentWind Characteristics over Terrain with Mixed Surface Roughness", *Radiation Protection Dosimetry*, Vol. 73, No. 1-4, pp. 257-260.

Astrup, P., T. Mikkelsen, and S. Deme, 2001, "METRODOS: Meteorological Preprocessor Chain", *Physics and Chemistry of the Earth, Part B: Hydrology, Oceans, and Atmosphere*, Vol. 26, No. 2, pp. 105-110.

Barry, R.G. and R.J. Chorley, 1968, *Atmosphere, Weather and Climate*, Butler and Tanner, London.

Belcher, S. E. D. P. Xu, and J. C. R. Hunt, 1990, "The Response of a Turbulent Boundary Layer to Arbitrarily Distributed Two-Dimensional Roughness Changes", *Quarterly Journal of the Royal Meteorological Society*, Vol. 116, pp. 611-635.

Bridger, A.F.C., A.J. Becker, F.L.Ludwig, and R.M.Endlich, 1994, "Evaluation of WOCSS Wind Analysis Scheme for the San Francisco Bay Area", *Journal of Applied Meteorology*, Vol.33, pp. 1210-1218.

Bhumralkar, C. M., R. L. Mancuso, F. L. Ludwig, and D. S. Renné, 1980, "A Practical and Economic Method for Estimating Wind Characteristics at Potential Wind Energy Conversion Sites", *Solar Energy*, Vol. 25, No. 1, pp. 55-65.

Carruthers, D. J., J. C. R. Hunt, and W.S. Weng, 1988, "A Computational Model of Stratified Turbulent Air Flow over Hills—FLOWSTAR I", *Computer Techniques in Environmental Studies: Proceedings of Envirosoft 88, 2nd International Conference,* Porto Carras, Greece, pp. 481-492.

Dawson, R., 2005, *Introduction to Atmospheric Physics*, http://www.ldeo.columbia.edu/dees/ees/climate/lectures/radiation/

Endlich, R. M., 1967, "An Iterative Method for Altering the Kinematic Properties of Wind Fields", *Journal of Applied Meteorology*, Vol. 6, pp. 837-844.

Endlich, R. M., F. L. Ludwig, C. M. Bhumralkar, and M. A. Estoque, 1982, "A Diagnostic Model for Estimating Winds at Potential Sites for Wind Turbines", *Journal of Applied Meteorology*, Vol. 21, No. 10, pp. 1441-1454.

Endlich, R. M., 1984, "Wind Energy Estimates by Use of a Diagnostic Model", *Boundary-Layer Meteorology*, Vol. 30, pp. 375-386.

Finardi, S., G. Brusasca, M.G. Morselli, F. Trombetti, and F. Tampieri, 1993, "Boundary-Layer Flow over Analytical Two-Dimensional Hills: A Systematic Comparison of Different Models with Wind Tunnel Data", *Boundary-Layer Meteorology*, Vol. 63, No. 3, pp. 259-291.

Goodin, W. R., G. J. McRae, and J.H. Seinfeld, 1979, "A Comparison of Interpolation Methods for Sparse Data: Application to Wind and Concentration Fields", *Journal of Applied Meteorology*, Vol. 18, pp. 761-771.

Goodin, W. R., G. J. McRae, and J.H. Seinfeld, 1980, "An Objective Analysis Technique for Constructing Three-Dimensional Urban-Scale Wind Fields", *Journal of Applied Meteorology*, Vol. 19, pp. 98-108.

Hess S.L., 1966, *Introduction to Theoretical Meteorology*, Holt, Rinehart and Winston, New York.

Homicz, G.F., 2002, "Three-Dimensional Wind Field Modeling:A Review", Sandia National Laboratories.

Hunt, J.C.R. and K.J., Richards, 1984, "Stratified Airflow over One or Two Hills", *Boundary-Layer Meteorology*, Vol. 30, pp. 223-259.

Hunt, J.C.R., K. J. Richards, and P.W.M. Brighton, 1988a, "Stably Stratified Shear Flow Over Low Hills," *Quarterly Journal of the Royal Meteorological Society*, Vol. 114, pp. 859-886.

Hunt, J.C.R., S. Leibovich, and K.J.Richards, 1988b, "Turbulent Shear Flows Over Low Hills", *Quarterly Journal of the Royal Meteorological Society*, Vol. 114, pp. 1435-1470.

Hunt, J.C.R., and W. Snyder, 1980, "Experiments on Stably and Neutrally Stratified Flow Over a Model Three-Dimensional Hill", *Journal of Fluid Mechanics*, Vol. 96, pp. 671-704.

Jackson, P.S. and J.C.R. Hunt, 1975, "Turbulent Wind Flow Over a Low Hill", *Quarterly Journal of the Royal Meteorological Society*, Vol. 101, pp. 929-955.

Kitada, T., A. Kaki, H. Ueda, and L.K. Peters, 1983, "Estimation of Vertical Air Motion from Limited Horizontal Wind Data—A Numerical Experiment", *Atmospheric Environment*, Vol. 17, No. 11, pp. 2181-2192.

Kleissl, J., *et al.*, 2004, *Analysis and Application of Sheppard's Airflow Model to Predict Mechnical orographic Lifting and the Occurance of Mountain Clouds,* Michigan Technological University.

Liu, C. Y. and W. R. Goodin, 1976, "An Iterative Algorithm for Objective Wind Field Analysis", Monthly Weather Review, Vol. 104, pp. 784-792.

Ludwig F.L., J.M. Livingston, and R.M. Endlich, 1991, "Use of Mass Conservation and Critical Dividing Streamline Concepts for Efficient Analysis of Winds in Complex Terrain", *Journal of Applied Meteorology*, Vol. 30, pp. 1490-1499.

Ludwig F.L., D. Sinton, 2000, "Evaluating an Objective Wind Analysis Technique with a Long Record of Routinely Collected Data", *American Meteorological Society*, Vol.39, pp.335-347.

Marshall, J., and A. Plumb, 2004, "Circulation of the Atmosphere and Ocean: An Introductory Text", Massachusetts Institute of Technology.

Mason, P. J. and J. C. King, 1985, "Measurements and Predictions of Flow and Turbulence over an Isolated Hill of Moderate Slope," *Quarterly Journal of the Royal Meteorological Society*, Vol. 111, pp. 617–640.

Mason, P. J. and R. I. Sykes, 1979, "Flow over an Isolated Hill of Moderate Slope", *Quarterly Journal of the Royal Meteorological Society*, Vol. 105, pp. 383-395.

Mikkelsen, T., S. Thykier-Nielsen, P. Astrup, M. Santabárbara, J.H. Srensen, A. Rasmussen, L. Robertson, A. Ullerstig, S. Deme, R. Martens, J.G. Bartzis, and J. Päsler-Sauer, 1997, "MET-RODOS: A Comprehensive Atmospheric Dispersion Module," *Radiation Protection Dosimetry*, Vol. 73, Nos. 1-4, pp. 45-56.

Radiosonde Database Access, http://raob.fsl.noaa.gov.

Ratto, C. F., R. Festa, C. Romeo, O.A. Frumento, and M. Galluzzi, 1994, "Mass-Consistent Models forWind FIelds over Complex Terrain: The State of the Art", *Environmental Software*, Vol. 9, No. 4, pp. 247-268.

Reynolds, S. D., P.M. Roth, and J.H. Seinfeld, 1973, "Mathematical Modeling of Photochemical Air Pollution—I", *Atmospheric Environment*, Vol. 7, pp. 1033-1061.

Ross, D. G., I.N. Smith, P.C. Manins, and D.G. Fox, 1988, "Diagnostic Wind Field Modeling for Complex Terrain: Model Development and Testing", *Journal of Applied Meteorology*, Vol. 27, pp. 785-796.

Sasaki, Y.,1958, "An Objective Analysis Based on the Variational Method," *Journal of the Meteorological Society of Japan*, Vol. 36, No. 3, pp. 77-88.

Sasaki, Y.,1970a, "Numerical Variational Analysis Formulated Under the Constraints a, Determined by Longwave Equations and a Low-Pass Filter," *MonthlyWeather Review*, Vol. 98, No. 12, pp. 884-898.

Sasaki, Y.,1970b, "Some Basic Formalisms in Numerical Weather Analysis," *Monthly Weather Review*, Vol. 98, No. 12, pp. 875-883.

Schmid, J., 1995, "Photovoltaik: ein Leitfaden für die Praxis; ein Informationspaket", *Köln: Verl. TÜV Rheinland*, pp. 10-12.

Sherman, C. A., 1978, "A Mass-Consistent Model for Wind Fields over Complex Terrain", *Journal of Applied Meteorology*, Vol. 17, pp. 312-319.

Sheppard, P.A., 1956, "Air Flow over Mountains", *Quarterly Journal of the Royal Meteorological Society*, Vol. 82, pp. 528–529.

Smith, R., 1980, "Linear Theory of Stratified Hydrostatic Flow Past an Isolated Mountain", *Tellus*, Vol.32, pp.348-364.

Sutton. O.G., 1953, *Micrometeorology*, McGraw-Hill Inc.

Taylor, F.T., 1954, *Elementary Meteorology*, Prentice-Hall, New York.

Taylor, P. A., J.L. Walmsley, and J.R. Salmon, 1983, "A Simple Model of Neutrally Stratified Boundary-Layer Flow over Real Terrain Incorporating Wavenumber Dependent Scaling", *Boundary-Layer Meteorology*, Vol. 26, No. 2, pp. 169-189.

Troen, I. and A.,de Baas, 1986, "A Spectral Diagnostic Model for Wind Flow Simulation in Complex Terrain", in *Proceedings of the European Wind Energy Association Conference and Exhibition,* Rome, Italy, October 7–9, pp. 243–249.

Walmsley, J. L., P.A. Taylor, and T. Keith, 1986, "A Simplified Model of Neutrally Stratified Boundary-Layer Flow over Complex Terrain with Surface Roughness Modulations (MS3DJH/3R)", *Boundary-Layer Meteorology*, Vol. 36, pp. 157-186.

Wenham, S.R., M.A. Green, M.E. Watt, 1998, *Applied Photovoltaics*, pp. 1-19.

United States of Geographical Survey, http://www.usgs.gov/pubprod/digitaldata.html.